Cell Reports

Article

C-Terminal Motifs of the MTW1 Complex Cooperatively Stabilize Outer Kinetochore Assembly in Budding Yeast

Graphical Abstract

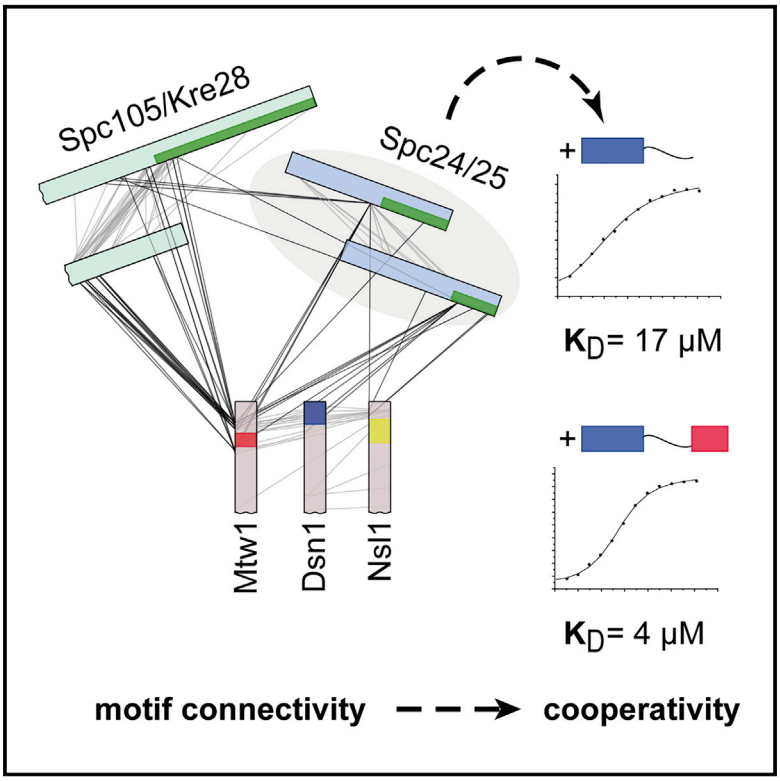

Authors

Medini Ghodgaonkar-Steger, Mia Potocnjak, Tomasz Zimniak, ..., David Jan Drexler, Gregor Witte, Franz Herzog

Correspondence

herzog@genzentrum.lmu.de

In Brief

The kinetochore links chromosomes to spindle microtubules and has to withstand the pulling forces of depolymerizing microtubules to segregate chromosomes during cell division. Using chemical crosslinking and mass spectrometry, Ghodgaonkar-Steger et al. identify the protein motifs that cooperatively stabilize the 10-subunit outer kinetochore network that forms the microtubule binding site.

Highlights

- XL-MS of native kinetochore complexes identifies KMN subunit connectivity in yeast
- Two C-terminal MTW1 subunit motifs recruit SPC105 complex through Kre28
- C-terminal MTW1 motifs cooperatively stabilize the KMN network
- Cooperative assembly of the KMN network is enhanced by NDC80-SPC105 association

Ghodgaonkar-Steger et al., 2020, Cell Reports *32*, 108190
September 29, 2020
https://doi.org/10.1016/j.celrep.2020.108190

CellPress

Cell Reports

CellPress
OPEN ACCESS

Article

C-Terminal Motifs of the MTW1 Complex Cooperatively Stabilize Outer Kinetochore Assembly in Budding Yeast

Medini Ghodgaonkar-Steger,[1,2] Mia Potocnjak,[1,2] Tomasz Zimniak,[1] Josef Fischböck-Halwachs,[1] Victor Solis-Mezarino,[1] Sylvia Singh,[1] Tea Speljko,[1] Götz Hagemann,[1] David Jan Drexler,[1] Gregor Witte,[1] and Franz Herzog[1,3,*]

[1]Gene Center Munich and Department of Biochemistry, Ludwig-Maximilians-Universität München, Feodor-Lynen-Str. 25, 81377 Munich, Germany

[2]These authors contributed equally

[3]Lead Contact

*Correspondence: herzog@genzentrum.lmu.de

https://doi.org/10.1016/j.celrep.2020.108190

SUMMARY

Kinetochores are macromolecular protein assemblies at centromeres that mediate accurate chromosome segregation during cell division. The outer kinetochore KNL1^{SPC105}, MIS12^{MTW1}, and NDC80^{NDC80} complexes assemble the KMN network, which harbors the sites of microtubule binding and spindle assembly checkpoint signaling. The buildup of the KMN network that transmits microtubule pulling forces to budding yeast point centromeres is poorly understood. Here, we identify 225 inter-protein crosslinks by mass spectrometry on KMN complexes isolated from *Saccharomyces cerevisiae* that delineate the KMN subunit connectivity for outer kinetochore assembly. C-Terminal motifs of Nsl1 and Mtw1 recruit the SPC105 complex through Kre28, and both motifs aid tethering of the NDC80 complex by the previously reported Dsn1 C terminus. We show that a hub of three C-terminal MTW1 subunit motifs mediates the cooperative stabilization of the KMN network, which is augmented by a direct NDC80-SPC105 association.

INTRODUCTION

In eukaryotes, the kinetochore mediates the faithful distribution of the genetic material to daughter cells during each cell division. The kinetochore is a macromolecular protein complex that assembles at specialized chromatin regions called centromeres and connects chromosomes to spindle microtubules. In budding yeast, the kinetochore is built on point centromeres, a specific DNA sequence of ~125 bp wrapped around a single Cse4-containing nucleosome, the budding yeast ortholog of the human histone H3 variant CENP-A (the human orthologs are superscripted if appropriate). By contrast, the human kinetochore is assembled on regional centromeres that span over megabases of DNA containing ~200 CENP-A nucleosomes (Bodor et al., 2014; Pluta et al., 1995). The core structure and function of the kinetochore are largely conserved between budding yeast and humans but differ in terms of complexity and size (Cheeseman and Desai, 2008; Joglekar et al., 2009; Santaguida and Musacchio, 2009; van Hooff et al., 2017). The kinetochore architecture can be subdivided into the outer kinetochore that constitutes the microtubule binding interface and the inner kinetochore that is assembled at centromeric chromatin by the constitutive centromere-associated network (CCAN) or CTF19 complex (CTF19c) in budding yeast (Cheeseman and Desai, 2008).

The essential inner kinetochore proteins Mif2^{CENP-C} and Ame1/Okp1 bind to the C- and N-terminal domains of Cse4^{CENP-A} (Anedchenko et al., 2019; Fischboeck et al., 2018; Westermann et al., 2003; Xiao et al., 2017), respectively, and to the MTW1^{MIS12} complex (Dimitrova et al., 2016; Przewloka et al., 2011; Screpanti et al., 2011), serving as direct links between the outer kinetochore and the centromeric nucleosome.

In all eukaryotes, the outer kinetochore is built up by the 10-subunit KMN network that is assembled by three distinct subcomplexes: the SPC105^{KNL1} complex including the subunits Spc105^{KNL1} and Kre28^{ZWINT}; the MTW1^{MIS12} complex (MTW1c^{MIS12c}) comprising the subunits Mtw1^{MIS12}, Dsn1^{DSN1}, Nsl1^{NSL1}, and Nnf1^{PMF1}; and the NDC80^{NDC80} complex composed of Ndc80^{NDC80}, Nuf2^{NUF2}, Spc24^{SPC24}, and Spc25^{SPC25}.

The NDC80c contributes the essential microtubule binding activity of the KMN network (Cheeseman et al., 2006; Ciferri et al., 2008; Wei et al., 2007) constituted by two calponin homology domains in Ndc80 and Nuf2 and the basic Ndc80 N-terminal tail (Guimaraes et al., 2008; Miller et al., 2008). At the opposite end, RWD (RING finger- and WD-repeat-containing proteins and DEAD-like helicases) domains within the Spc24/25 dimer mediate kinetochore targeting of the microtubule-binding subunits through their interaction with the MTW1c^{MIS12c} (Malvezzi et al., 2013; Petrovic et al., 2010). Ndc80 also binds the yeast-specific DASH/Dam1 complex, which is an essential microtubule-binding complex in budding yeasts (Cheeseman et al., 2001; De Wulf et al., 2003; Westermann et al., 2006; Lampert et al., 2013).

Crystal structures of human (Petrovic et al., 2016) and *Kluyveromyces lactis* (Dimitrova et al., 2016) MTW1^{MIS12} complexes show that its four subunits are assembled as two heterodimers whose C and N termini are organized at opposite ends. The N-terminal head domain formed by Mtw1^{MIS12} and Nnf1^{PMF1} interacts with the N termini of Mif2^{CENP-C} (Petrovic et al., 2016; Przewloka et al., 2011; Screpanti et al., 2011) and Ame1 (Dimitrova et al., 2016; Hornung et al., 2011). Biochemical data showed that the C terminus of Dsn1 is required for recruiting the NDC80c (Dimitrova et al., 2016; Kudalkar et al., 2015; Malvezzi et al., 2013) in budding yeasts and that the C termini of Mtw1 and Nsl1 aid in stabilizing this interaction (Kudalkar et al., 2015). Crystal structures of the Dsn1 peptide or a Cnn1 helical peptide in complex with the globular Spc24/25 RWD domains revealed the same binding mode of these two NDC80c recruiters (Bock et al., 2012; Dimitrova et al., 2016; Malvezzi et al., 2013; Schleiffer et al., 2012; Wei et al., 2006). Similarly, the human ortholog of Cnn1, CENP-T, has been identified as docking site for the NDC80c (Gascoigne et al., 2011; Nishino et al., 2013). The role of Cnn1 in bridging NDC80c to the centromere becomes crucial in cells where the MTW1c function is compromised (Hornung et al., 2014; Lang et al., 2018; Rago et al., 2015).

A comparison of the reported protein contacts linking the subcomplexes of the KMN network in humans and budding yeast indicates similarities and differences in assembly that are largely based on the varying length and sequences of the C-terminal tails extending from the coiled-coil (CC) shaft of the orthologous MTW1c^{MIS12c} subunits (Dimitrova et al., 2016; Petrovic et al., 2010, 2014, 2016). In humans, two motifs within the C-terminal NSL1 tail, which are not conserved in budding yeast, are required for binding the NDC80c and KNL1c. The C-terminal NSL1$^{258–281}$ motif was sufficient to establish a tight interaction with the homodimeric RWD domains of KNL1 (Petrovic et al., 2010, 2014) in the absence of its binding partner ZWINT, whereas the PVIHL motif (NSL1$^{209–213}$) is necessary for binding NDC80c, but a high-affinity MIS12c-NDC80c interaction likely requires additional contacts (Petrovic et al., 2010).

The Spc105^{KNL1} N terminus serves as an assembly platform for spindle checkpoint proteins (London et al., 2012; Shepperd et al., 2012; Yamagishi et al., 2012), but how the SPC105c is recruited to the KMN network in *Saccharomyces cerevisiae* has not yet been addressed.

The inability to capture flexible and disordered regions and the difficulty to analyze full-length assemblies larger than individual subcomplexes have limited a comprehensive description of the kinetochore architecture. The mass spectrometric identification of chemical crosslinks (XL-MS) has been developed to study the protein connectivity of native or *in vitro*-reconstituted protein complexes (Herzog et al., 2012; Walzthoeni et al., 2012).

We present a comprehensive protein connectivity map of the native budding yeast outer kinetochore. The detection of several crosslinks to the Mtw1 C terminus indicates the importance of this region and identifies a predicted helical motif. We show that the C-terminal helical motifs of Mtw1 and Nsl1 synergistically interact with the Spc105/Kre28 complex, whereas the Spc24/25 heterodimer is recruited through association with the Dsn1, Nsl1, and Mtw1 C termini. Moreover, we demonstrate *in vitro* that, in contrast to humans, the C-terminal homodimeric RWD domains of Spc105 are dispensable for the recruitment of the SPC105c to the KMN network and that this interaction is mediated, in part, through the predicted CC domain of Kre28. Our *in vitro* reconstitution assays identify the molecular basis of the cooperative assembly of the SPC105c and NDC80c onto the MTW1c C termini that is further stabilized by a weak SPC105c-NDC80c association.

RESULTS

A Protein Connectivity Map of the KMN Network

To obtain a complete map of protein-protein contacts of the budding yeast outer kinetochore, we performed large-scale purifications of endogenously 6xHis-6xFLAG-tagged kinetochore proteins from *S. cerevisiae* (Figure 1A; Table S1). The quantitative mass spectrometric analysis of the Dsn1 purification yielded a nearly stoichiometric 10-subunit KMN network (Akiyoshi et al., 2010), low abundant CTF19 subcomplexes such as COMA (Ctf19/Okp1/Mcm21/Ame1) (Hornung et al., 2014), and subunits of the DASH/Dam1 complex. Isolation of Cnn1 and Wip1 coprecipitated Mcm16/Ctf3/Mcm21, Chl4/Iml3, and COMA complexes, whereas the KMN subunits were predominantly low abundant (Figure 1A). In reciprocal purifications of Mcm16 and Ctf3, the CTF19 subcomplexes Cnn1/Wip1, COMA, and Chl4/Iml3 were enriched over the KMN proteins, in agreement with previous studies indicating that direct interaction with Mcm16/Ctf3/Mcm21$^{CENP-H/I/K}$ anchors Cnn1/Wip1$^{CENP-T/W}$ through Chl4/Iml3$^{CENP-N/L}$ at the inner kinetochore and that Mcm16/Ctf3/Mcm21$^{CENP-H/I/K}$ has a direct role in recruiting NDC80c in a Cnn1^{CENP-T}-dependent manner (Basilico et al., 2014; Kim and Yu, 2015; Pekgöz Altunkaya et al., 2016).

In order to map the protein connectivity, we performed XL-MS analysis of the purified native kinetochore complexes. In total, we identified 225 inter-protein and 237 intra-protein crosslinks on the KMN network and its associated CTF19c subunits (Figure 1B; Tables S4 and S5). The majority of the detected crosslinks in our native kinetochore network is in agreement with previous studies (Hornung et al., 2011, 2014; Kudalkar et al., 2015; Maskell et al., 2010). Crosslinks between Mcm16/Ctf3/Mcm21 and Cnn1 correspond to crosslinks recently reported on *in vitro*-reconstituted complexes (Pekgöz Altunkaya et al., 2016) and are consistent with the structure of the Spc24/25 RWD dimer bound to the Cnn1$^{60–84}$ N-terminal peptide (Lang et al., 2018; Malvezzi et al., 2013; Schleiffer et al., 2012). The crosslink-derived restraints are also in agreement with the crystal structure of the *K. lactis* MTW1c (Dimitrova et al., 2016) and indicate that the C termini of Mtw1, Nsl1, and Dsn1 are in close proximity, forming a hub of tightly aligned helical motifs (Figures 1B and 2A). In particular, our connectivity map pinpointed the Mtw1 C terminus as the central site for building up the KMN network. Several crosslinks in the Mtw1 C terminus indicated that Spc105/Kre28 is recruited through the C-terminal part of Spc105 and the predicted CC of Kre28 and that NDC80c is bound through the RWD domains of Spc24/25 (Kudalkar et al., 2015) (Figure 1B; Tables S4 and S5).

Furthermore, we recombinantly expressed the 10-subunit KMN network from a single baculovirus in insect cells (Weissmann et al., 2016) and purified a stoichiometric KMN super-complex to homogeneity (Figure S1A). The XL-MS analysis of the

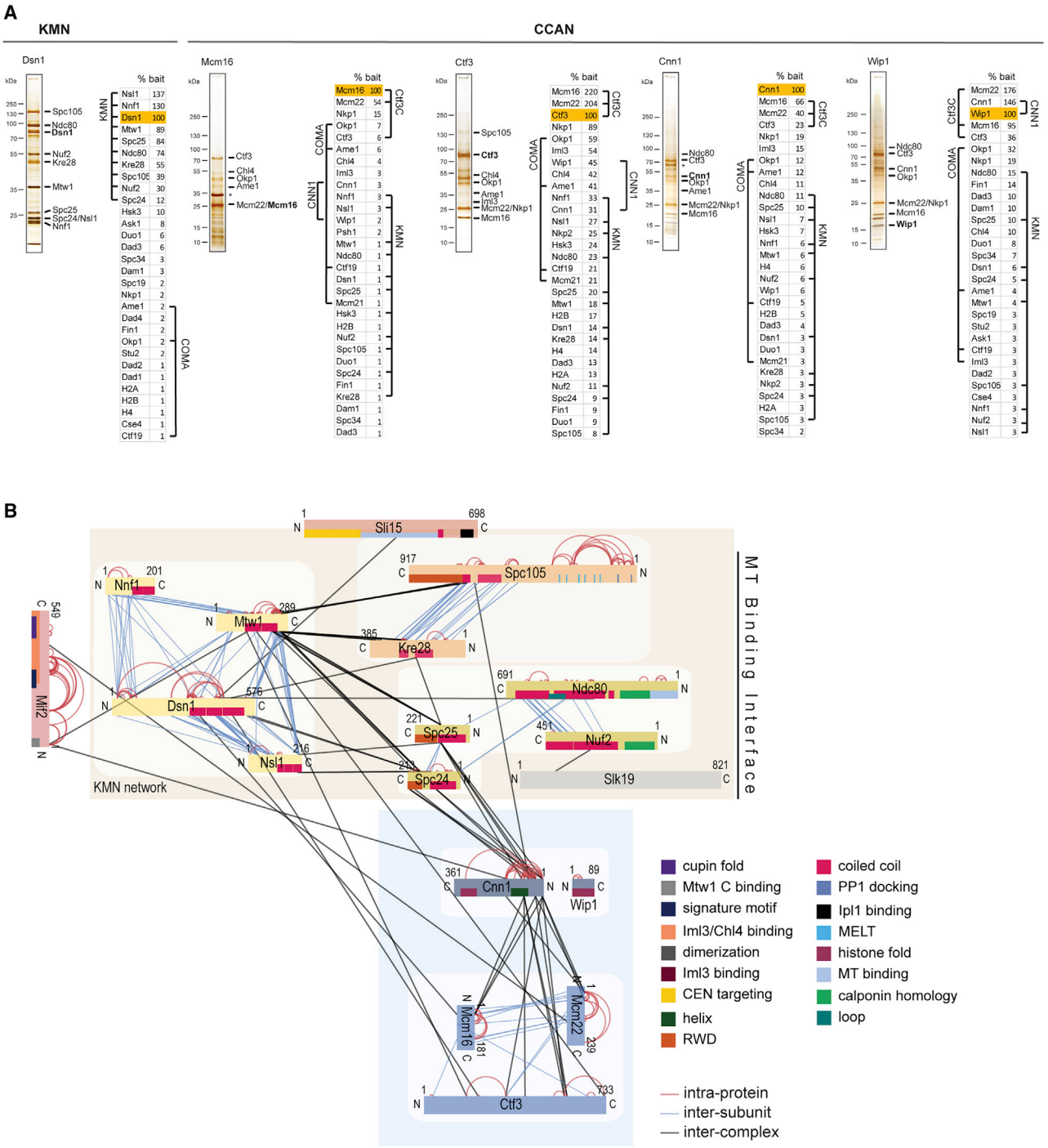

Figure 1. Subunit Connectivity of the Native Budding Yeast Outer Kinetochore Based on Crosslink-Derived Spatial Restraints

(A) The indicated kinetochore proteins were endogenously 6xHis-6xFLAG tagged and affinity purified using anti-FLAG magnetic beads from yeast cell extracts. The eluted proteins were visualized by SDS-PAGE and silver staining and subjected to mass spectrometric analysis before and after crosslinking. Protein intensities detected by mass spectrometry were normalized to the bait, and their relative abundance to the bait is indicated. Proteins were annotated on the SDS-PAGE, with asterisk (*) indicating contaminants.

(B) Schematic representation of 225 inter-protein and 238 intra-protein crosslinks (Table S4) identified on 5 different kinetochore subcomplexes (shown in A) delineated the protein connectivity of the KMN network and its interactors. Proteins are represented as bars indicating annotated domains according to a color scheme (Table S5), and subunits of a complex are shown in the same color. Protein lengths and crosslink sites are scaled to the amino acid sequence.

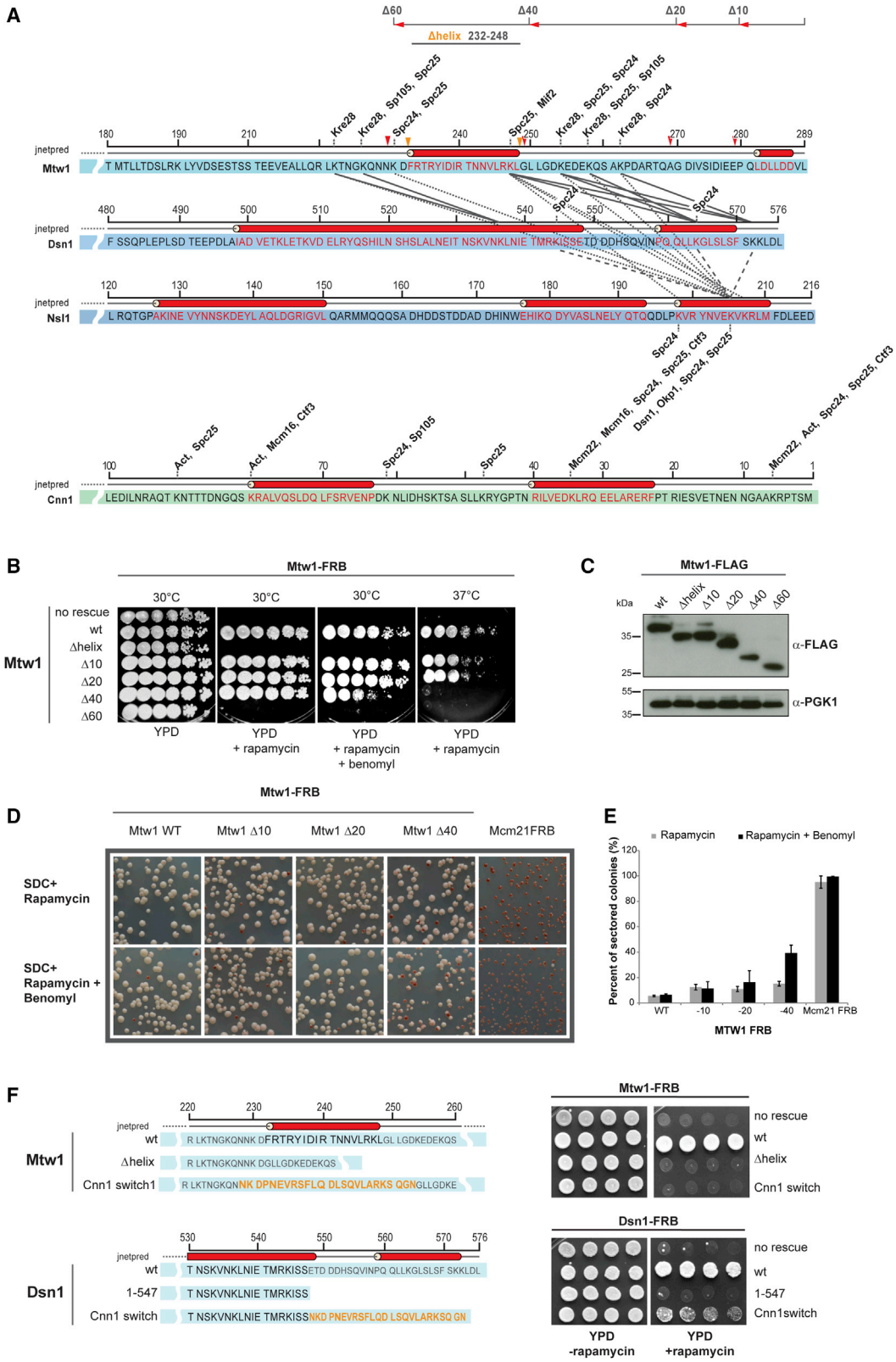

(legend on next page)

recombinant KMN network identified 191 inter-protein crosslinks (Figure S1B; Table S6) that confirmed the crosslinks on the native KMN network preparations but showed additional restraints connecting the C-terminal CC domain of Spc105 to the CCs of Ndc80 and Spc24/25.

Multiple C Termini of the MTW1 Complex Create a Hub for the KMN Network Assembly

Inter-protein crosslinks between the C termini of Mtw1, Dsn1, and Nsl1 are collinear, suggesting that the tails are aligned and protrude from one end of the MTW1c CC shaft (Dimitrova et al., 2016) (Figure 2A). Consistent with previous reports, we observed crosslinks from the C termini of Dsn1 and Nsl1 to lysine residues in the globular heads and the following CC extensions of Spc24/25. Crosslinks from Dsn1 and Nsl1 as well as from Spc24/25 and Spc105/Kre28 intersected close to a region of Mtw1 (residues 232–248) predicted to be a short helix (Figure 2A; Figure S2A). The flanking sequences of this putative Mtw1 helix were crosslinked to lysine residues within the CC domains of Spc105/Kre28 and Spc24/25 (Figures 1B and 2A; Table S4). The SPC105c was not crosslinked to the Nsl1 C terminus, which has been previously shown to tether KNL1c to the human KMN network (Petrovic et al., 2010, 2014). Nine crosslinks between the Cnn1 N terminus and Spc24/25 were validated by previous studies showing that Cnn1 competes with Dsn1 for Spc24/25 binding (Bock et al., 2012; Malvezzi et al., 2013; Schleiffer et al., 2012) and is the major site of Spc24/25 interaction (Figure 2A). Notably, a crosslink between the Cnn1 N terminus and the Spc105 CC region (residues 551–711) indicated a putative association of Cnn1 with the SPC105c.

Our XL-MS data suggest that helical motifs within the C termini of Mtw1, Dsn1, and Nsl1 are tightly aligned, providing a hub for interactions in order to cooperatively stabilize the KMN assembly.

The Short Helical Motif in the Mtw1 C Terminus Is Essential for Cell Survival

To address whether Mtw1 has a unique role in KMN assembly, we generated Mtw1 mutants lacking the helical motif (Mtw1-Δhelix or Mtw1Δ232–248) or the C-terminal 20, 40, or 60 amino acids (aa; Mtw1Δ20, Mtw1Δ40, or Mtw1Δ60, respectively). As the deletion of Mtw1 is lethal in budding yeast (Goshima and Yanagida, 2000), we used the anchor-away technique to conditionally remove the endogenous Mtw1-FRB from the nucleus by addition of rapamycin (Haruki et al., 2008) and ectopically express Mtw1 wild-type or mutant rescue alleles. The lethal phenotype could be rescued by expression of Mtw1 wild type (Figure 2B), and C-terminal truncations lacking up to 40 amino acids (Mtw1Δ10, Mtw1Δ20, and Mtw1Δ40) did not affect cell growth at 30°C. However, the expression of Mtw1Δ60 and Mtw1Δhelix did not rescue the lethal phenotype, indicating that the helical motif Mtw1$^{232–248}$ is essential for cell viability (Figures 2B and 2C). The Mtw1Δ40 mutant showed benomyl sensitivity and a temperature-sensitive growth defect at 37°C. To further corroborate the phenotype of the Mtw1Δ40 mutant, we performed a minichromosome loss assay (Figures 2B and 2D) (Hieter et al., 1985) by transforming an Mtw1 anchor-away strain with various Mtw1 rescue constructs and a centromeric plasmid carrying the SUP11 gene as a marker, which indicates minichromosome loss through red pigmentation. Whereas the Mtw1Δ10, Mtw1Δ20, and Mtw1Δ40 mutants showed only a minor increase in segregation defects compared with the wild-type Mtw1 on normal growth medium, the rate of missegregation was increased 5-fold for Mtw1Δ40 on benomyl-containing plates (Figures 2D and 2E). This indicated the functional relevance of amino acids 250–269 for the Mtw1 C terminus.

Dsn1 and Cnn1 have been shown to compete for the same binding site on the heterodimeric RWD domains of Spc24/25 (Bock et al., 2012; Malvezzi et al., 2013; Schleiffer et al., 2012). The short helices of Dsn1$^{560–571}$ and Cnn1$^{65–79}$ (Figure S2A) insert into the same hydrophobic cleft of the Spc24/25 RWD dimer (Dimitrova et al., 2016; Malvezzi et al., 2013). Moreover, a helix-switch assay substituting the last 29 amino acids of Dsn1 with the Cnn1$^{65–84}$ helical motif rescued cell death upon deletion of the Dsn1 C terminus (Dsn1$^{1–547}$) (Malvezzi et al., 2013). Similarly, we investigated whether substitution of the Mtw1$^{232–248}$ helix with the Cnn1$^{60–84}$ peptide rescued lethality of the Mtw1Δhelix mutant (Figure 2F). Replacing the Mtw1 residues 229–248 with Cnn1$^{60–84}$ did not rescue the growth defect, whereas the C-terminal fusion of Cnn1$^{60–84}$ to Dsn1$^{1–547}$ could partially rescue the lethal phenotype of Dsn1$^{1–547}$ (Figure 2F) (Malvezzi et al., 2013). This result indicated that the Mtw1 and Dsn1 helices execute non-redundant functions. The fact that substitution of the Mtw1$^{232–248}$ helix by Cnn1$^{60–84}$ was lethal suggested that the binding partner or site is different to that of the Dsn1 and Cnn1 helical peptides.

Deletion of the Mtw1$^{232–248}$ Helix Affects the Assembly of the Outer and Inner Kinetochore

Our XL-MS and *in vivo* experiments suggested that the Mtw1$^{232–248}$ helix mediated association of the NDC80c and SPC105c. To address the contribution of the Mtw1$^{232–248}$ helix to kinetochore assembly in the cell, we affinity purified

Figure 2. C-Terminal Motifs of the MTW1c Establish a Hub for the KMN Network Assembly

(A) Schematic representation of inter-protein crosslinks detected on the C-terminal tails of Mtw1, Dsn1, and Nsl1 and N-terminal tail of Cnn1. Predicted helical motifs are shown as red cylinders. Crosslinks from Dsn1 to Mtw1, from Nsl1 to Mtw1, or from Dsn1 to Nsl1 are indicated by bold, dotted, or dashed lines, respectively. Crosslinks from MTW1c subunits to other kinetochore proteins are indicated by black dotted vertical lines.

(B) Analysis of Mtw1 C-terminal deletion mutants in cell viability assays using the anchor-away technique. Mtw1-FRB strains harboring the indicated rescue alleles were spotted in serial dilutions on YPD, YPD + rapamycin, or YPD + rapamycin + benomyl plates and incubated at 30°C or 37°C.

(C) Western blot analysis of immunoprecipitated Mtw1-1xFLAG showed expression levels of the wild-type and mutant proteins. Pgk1 served as a loading control.

(D) Analysis of chromosomal segregation defect using a sectoring assay. MTW1 anchor-away strains were plated on synthetic defined complete media (SDC) + rapamycin or SDC + rapamycin + benomyl and grown at 30°C. A Mcm21-FRB strain served as a positive control.

(E) Quantification of the segregation assay performed in (D) displayed as mean ± standard deviation (SD) of 3 replicates.

(F) Growth assay analyzing the phenotype of the Mtw1/Cnn1 switch mutant where the Mtw1$^{232–248}$ helix was replaced by the Cnn1$^{60–84}$ helix in comparison with the previously published Dsn1 switch mutant (Malvezzi et al., 2013).

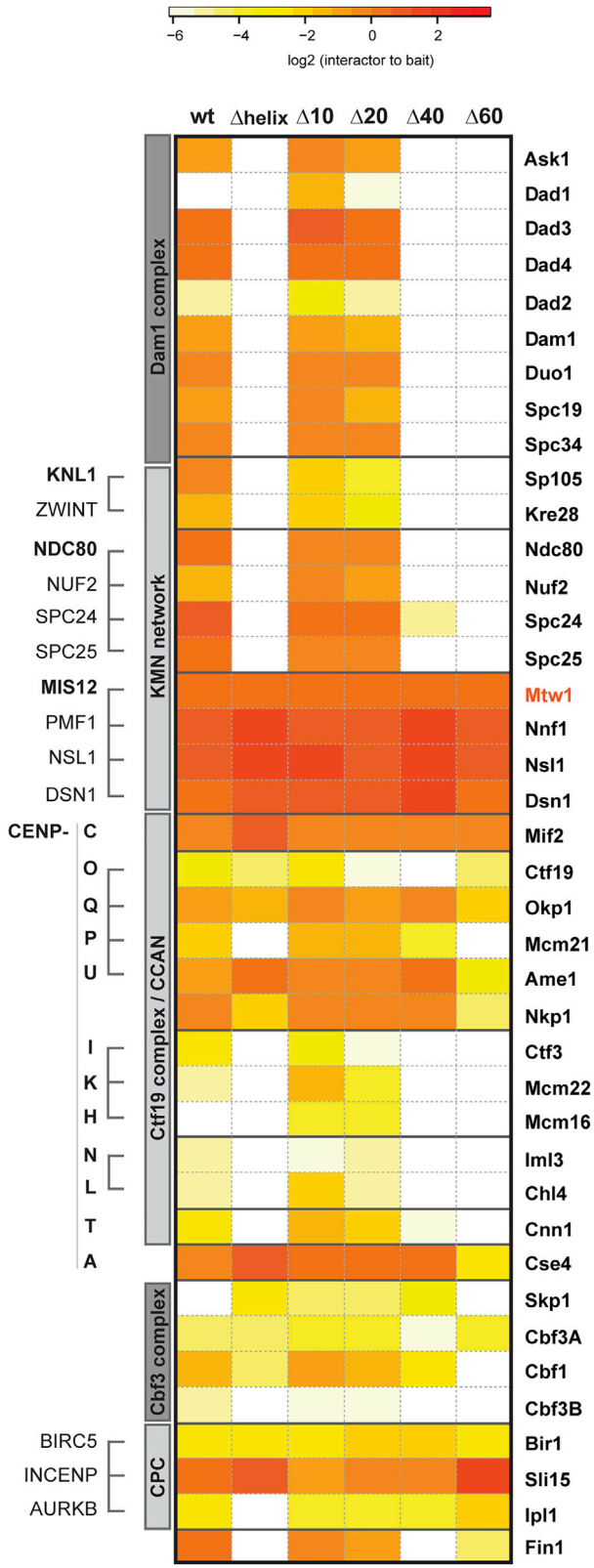

Figure 3. The Mtw1 C-Terminal Helix Is Critical for Outer Kinetochore Assembly

The heatmap summarizes the relative abundances of kinetochore proteins that copurified with the Mtw1 full-length (Kudalkar et al., 2015), the C-terminally truncated Mtw1 (Δ10, Δ20, Δ40, and Δ60), and the Mtw1Δhelix (Δ232–248) mutants. The 1xFLAG-tagged Mtw1 proteins were ectopically expressed in the Mtw1-FRB anchor-away background and purified from exponentially grown cells. Copurifying protein complexes were analyzed by mass spectrometry, and protein raw intensities were $\log_2$ transformed and normalized to the Mtw1 wild-type intensity. The mean of these ratios from 4 biological replicates is displayed according to the color scale.

ectopically expressed 1xFLAG-tagged Mtw1 wild-type and mutant (Mtw1Δ10, Mtw1Δ20, Mtw1Δ40, Mtw1Δ60, and Mtw1-Δhelix$^{232–248}$) proteins from whole-cell extracts and analyzed the complex composition by quantitative mass spectrometry (Figure 3). The Mtw1 mutant proteins did not affect formation of the tetrameric MTW1c and copurified similar levels of Mif2, Cse4, and subunits of the COMA complex. Truncation of the C-terminal 10 or 20 amino acids did not alter association of Mtw1 with kinetochore proteins. By contrast, the Mtw1-Δhelix$^{232–248}$, Mtw1Δ40, and Mtw1Δ60 mutants abrogated the interactions with the SPC105, NDC80, and DASH/Dam1 complexes and also affected the levels of the coprecipitated Mcm16/Ctf3/Mcm22 and Chl4/Iml3 complexes and of Cnn1. This is consistent with the finding that loss of NDC80c might destabilize Mcm16/Ctf3/Mcm22 and consequently affect the levels of associated Chl4/Iml3 and Cnn1 at the kinetochore (Basilico et al., 2014; Hinshaw and Harrison, 2019; Kim and Yu, 2015; Pekgöz Altunkaya et al., 2016). Although the helix$^{232–248}$ was present in the Mtw1Δ40 protein, the deletion of flanking C-terminal residues might compromise its integrity or weaken the interaction of NDC80c and SPC105c; thus, only residual levels of Spc24 were retained under the purification conditions. In summary, the Mtw1$^{232–248}$ helix is essential for the endogenous assembly of the KMN network and consequently may contribute to the cooperative stabilization of CTF19c subcomplexes at the kinetochore.

The Mtw1$^{232–248}$ Helical Peptide Is Required for the Interaction with the NDC80 and SPC105 Complexes

The crosslinking data identified several contacts between the Mtw1 C terminus and Spc105/Kre28 (Figures 1B and 2A), suggesting that it might be involved in recruiting Spc105/Kre28 to the KMN network. We performed peptide binding assays using a panel of Strep-tagged Cnn1$^{60–84}$, Mtw1$^{228–252}$, Dsn1$^{548–576}$, Nsl1$^{163–192}$, and Nsl1$^{183–216}$ helical peptides (Table S3) as baits in pull-down assays with recombinant Spc24/25 or Spc105/Kre28 complexes (Figure 4). Spc24/25 interacted with the Cnn1$^{60–84}$, Mtw1$^{228–252}$, and Dsn1$^{548–576}$ peptides. The Cnn1$^{60–84}$ peptide retained the highest levels of Spc24/25, which were significantly reduced for the Dsn1$^{548–576}$ and Mtw1$^{228–252}$ peptides. The two Nsl1 peptides Nsl1$^{163–192}$ and Nsl1$^{183–216}$ included the two C-terminal helical motifs of Nsl1 (Figure S2A). In our *in vitro* binding assay neither of the two Nsl1 peptides showed detectable binding of the Spc24/25 complex. An equimolar mixture of the Mtw1$^{228–252}$ and Dsn1$^{548–576}$ peptides retained higher levels of the Spc24/25 complex than achieved

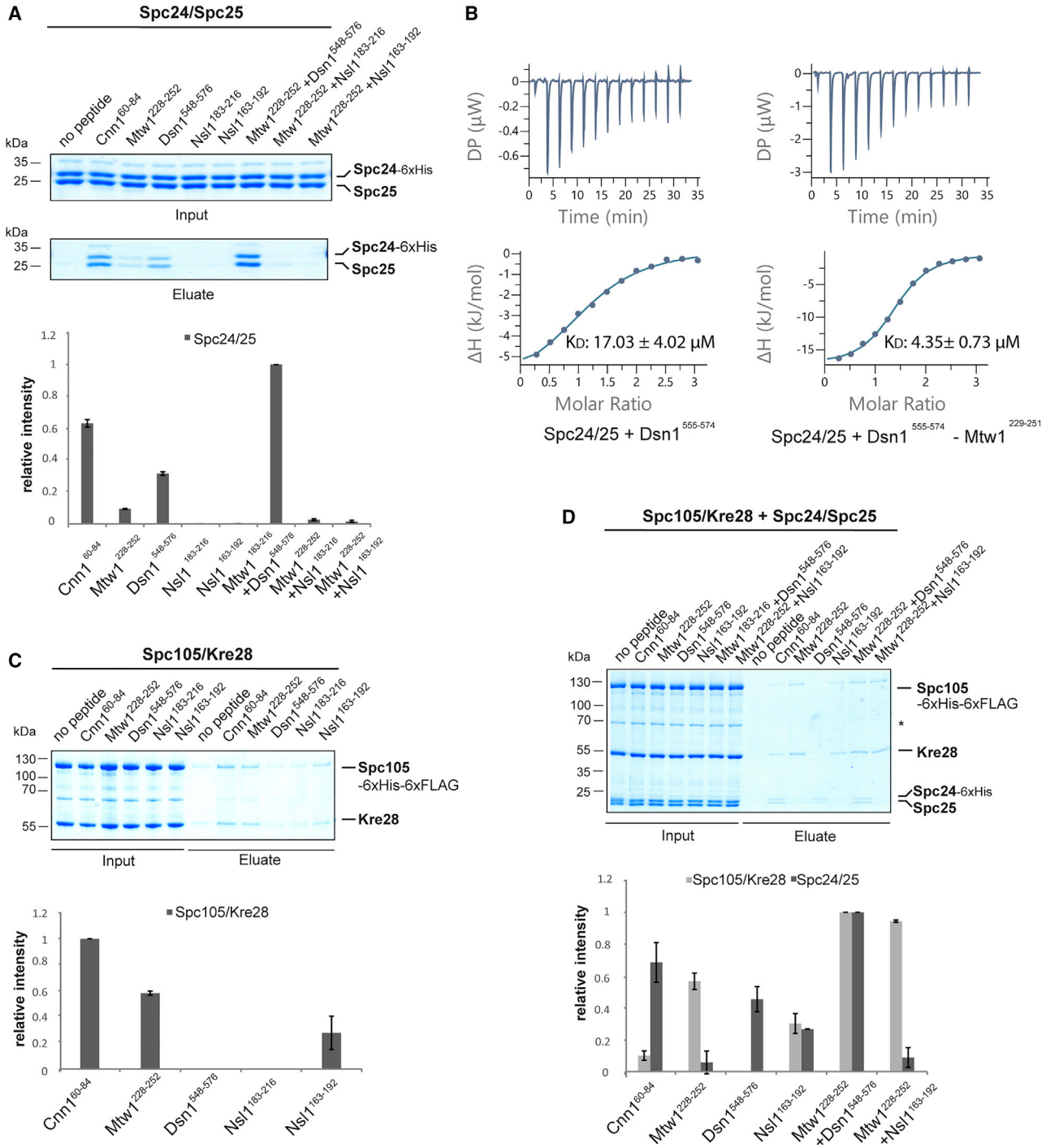

Figure 4. Motifs within the Mtw1, Dsn1, and Nsl1 C Termini and the Cnn1 N Terminus Show Different Relative Binding Affinities to Spc24/25 and Spc105/Kre28 Complexes *in Vitro*

(A) *In vitro* binding assay of Mtw1$^{228–252}$, Cnn1$^{60–84}$, Dsn1$^{548–576}$, Nsl1$^{183–216}$, or Nsl1$^{163–192}$ peptides to the Spc24/25 heterodimer. The 1xStrep-tagged peptides (Table S3) were incubated with recombinant Spc24/25 or Spc105/Kre28 at a molar ratio of 25:1. Bound complexes were isolated and eluted proteins were visualized by SDS-PAGE and Coomassie staining, respectively.

(B) Isothermal titration calorimetry with 51 μM Spc24-His/25 and 800 μM Dsn1$^{555–574}$ or Dsn1$^{555–574}$-Mtw1$^{229–251}$ peptide (Table S3).

(C) *In vitro* binding assay of Mtw1$^{228–252}$, Cnn1$^{60–84}$, Dsn1$^{548–576}$, Nsl1$^{183–216}$, or Nsl1$^{163–192}$ peptides to the Spc105/Kre28 complex analyzed as described in (A).

(legend continued on next page)

with the Dsn1$^{548–576}$ peptide alone, indicating an additive effect of Mtw1$^{228–252}$ and Dsn1$^{548–576}$ on the Spc24/25 interaction (Figure 4A). Accordingly, isothermal titration calorimetry (ITC) experiments of the Spc24/25 complex with the Dsn1$^{555–574}$ peptide alone or fused to the Mtw1$^{229–251}$ peptide (Table S3) resulted in an apparent dissociation constant (K_D) of 17.03 and 4.35 μM (Figure 4B), respectively. This confirmed the synergistic effect of both motifs on recruiting the NDC80c and is consistent with the observation that Cnn1 inhibits this interaction (Bock et al., 2012), as Cnn1$^{60–84}$ and Cnn1$^{1–270}$ showed a K_D value of 3.50 and 0.016 μM with Spc24/25, respectively (Malvezzi et al., 2013).

Recombinant Spc105/Kre28 was pulled down by the Cnn1$^{60–84}$ and Mtw1$^{228–252}$ peptides and was retained by the Nsl1$^{163–192}$ peptide to just above background levels (Figure 4C). In the presence of both Spc24/25 and Spc105/Kre28, Cnn1$^{60–84}$ exhibited higher relative affinity to Spc24/25, while Mtw1$^{228–252}$ preferentially bound Spc105/Kre28 (Figure 4D). Dsn1$^{548–576}$ exclusively isolated the Spc24/25 complex, and the equimolar mixture of Mtw1$^{228–252}$ and Dsn1$^{548–576}$ retained a nearly stoichiometric super-complex of Spc24/25 and Spc105/Kre28 at levels higher than pulled down by the individual peptides, suggesting a cooperative stabilization induced by the presence of the Mtw1$^{228–252}$ and Dsn1$^{548–576}$ peptides.

The Nsl1$^{163–192}$ peptide selectively bound Spc105/Kre28 and the mixture of Nsl1$^{163–192}$ and Mtw1$^{228–252}$ showed an increased relative affinity toward Spc105/Kre28, suggesting that Nsl1$^{163–192}$ cooperatively stabilized the Mtw1$^{228–252}$-Spc105/Kre28 interaction. This peptide binding assay indicated that the Mtw1$^{228–252}$ helical motif cooperatively stabilized the interactions of Dsn1$^{548–576}$ with the NDC80c and of Nsl1$^{163–192}$ with the SPC105c, which suggested that the Mtw1$^{228–252}$ helix is part of the interfaces for tethering NDC80c and SPC105c and that even at the level of isolated motifs the Mtw1$^{228–252}$ helix induces cooperative stabilization of the KMN network.

Cooperativity of Intra- and Inter-subcomplex Contacts Stabilizes the KMN Network

To investigate the recruitment of the NDC80c and SPC105c in the context of the full-length tetrameric MTW1c, we purified wild-type MTW1c composed of Mtw1, Nnf1, Nsl1, and 6xHis-1xStrep-Dsn1$^{171–576}$ (Hornung et al., 2011) and three mutant MTW1 complexes, including Mtw1Δhelix$^{232–248}$, Mtw1Δ60, and Dsn1$^{171–547}$, lacking the C-terminal 20 amino acids required for its interaction with Spc24/25 (Malvezzi et al., 2013). The recombinant MTW1 complexes were immobilized on streptavidin beads and incubated either with Spc24/25 or Spc105/Kre28, or both (Figure 5A). In agreement with the peptide binding assay, only the Mtw1 wild-type complex interacted with Spc24/25 (Figures 4A and 4C and 5A) (Dimitrova et al., 2016; Malvezzi et al., 2013). Notably, the Mtw1 helix motif was necessary for the interaction, as its deletion also abrogated Spc24/25 binding. Next, we addressed the requirement of the Mtw1 C terminus or Dsn1 C terminus for Spc105/Kre28 binding. Deletion of the Mtw1$^{232–248}$ helix reduced the isolated Spc105/Kre28 levels by more than half (Figures 5A and 5B), and truncation of the C-terminal 60 amino acids reduced Spc105/Kre28 to background levels.

In competitive binding assays in the presence of both Spc24/25 and Spc105/Kre28, we consistently observed a 2-fold increase in the bound Spc105/Kre28 levels (Figures 5A and 5B). Whether SPC105c and NDC80c interact in the absence of the MTW1c is unknown. We detected a crosslink between lysine-118 of Spc25 and lysine-199 of Kre28 in the native KMN network (Figure 1B; Table S4) and two and three crosslinks from recombinant Spc24 and Spc25, respectively, to Spc105 (Figure S1B; Table S6), which connected the CCs flanking the C-terminal RWD domains (Figure S2B) (Petrovic et al., 2014). Together with the two crosslinks between the CC regions of Ndc80 and Spc105 (Figure S1B; Table S6), these restraints suggested a direct association of the CC in Spc105/Kre28 and NDC80c. SEC and *in vitro* binding experiments indicated a weak Spc105/Kre28-Spc24/25 interaction by a shift of the Spc24/25 peak fraction in the presence of the Spc105/Kre28 complex (Figures S3A and S3B).

The *in vitro* binding assays using the wild-type and mutant MTW1c were in agreement with the peptide binding experiments and demonstrated the requirement of the putative Mtw1$^{232–248}$ helix for recruiting NDC80c and SPC105c and indicated cooperative stabilization of the KMN network through direct binding of NDC80c to SPC105c.

The Mtw1 Helix Residues 244–248 Mediate the Interaction with Spc24/25

To further narrow down the binding site of Spc105/Kre28 and Spc24/25 on the Mtw1$^{232–248}$ helix, we performed a multiple sequence alignment of the helix region from interrelated budding yeasts (Figure 5C). Based on this analysis, we generated point mutants of residues in either half of the helix (MTW1cMtw1$^{F232D/Y236D}$, MTW1cMtw1$^{R233D/Y236D}$, MTW1cMtw1$^{V244D/L248D}$) (Figures 5C–5F). In *in vitro* binding assays, the MTW1cMtw1$^{F232D/Y236D}$ mutant still bound Spc24/25 but showed reduced levels of associated Spc105/Kre28 (Figures 5D and 5E). In comparison, MTW1cMtw1$^{R233D/Y236D}$ retained similar levels of Spc105/Kre28 but showed further reduction of the bound Spc24/25 complex. Both the Mtw1Δhelix (Figures 5A and 5B) and the helix double point mutations showed more than 60% reduction in the Spc105/Kre28 binding compared with wild-type MTW1c, indicating that additional contacts may contribute to the cooperative stabilization. Notably, the two point mutations in the second helix half, Mtw1$^{V244D/L248D}$, abrogated Spc24/25 binding beyond the detection limit despite the presence of full-length Dsn1 (Figure 5D). In cell viability assays using the anchor-away method, Mtw1$^{F232D/Y236D}$ and Mtw1$^{R233D/Y236D}$, which displayed reduced levels of Spc24/25 binding, showed normal growth with a slight sensitivity to benomyl, whereas the expression of Mtw1$^{V244D/L248D}$ was lethal (Figures 5F and 5G). Taken together, the lethality caused upon mutation of the Mtw1 residues valine-244 and leucine-248

(D) *In vitro* competition assay of Spc105/Kre28 and Spc24/25 complexes for binding to the indicated peptides. Equimolar ratios of Spc105/Kre28 and Spc24/25 complexes were incubated with the immobilized peptides, and bound proteins were analyzed as described in (A). The bar charts in (A), (C), and (D) show the relative intensities of the bound proteins quantified by ImageJ (Schneider et al., 2012) and normalized to the most intense signal displayed as mean ± SD (n = 2).

CellPress
OPEN ACCESS

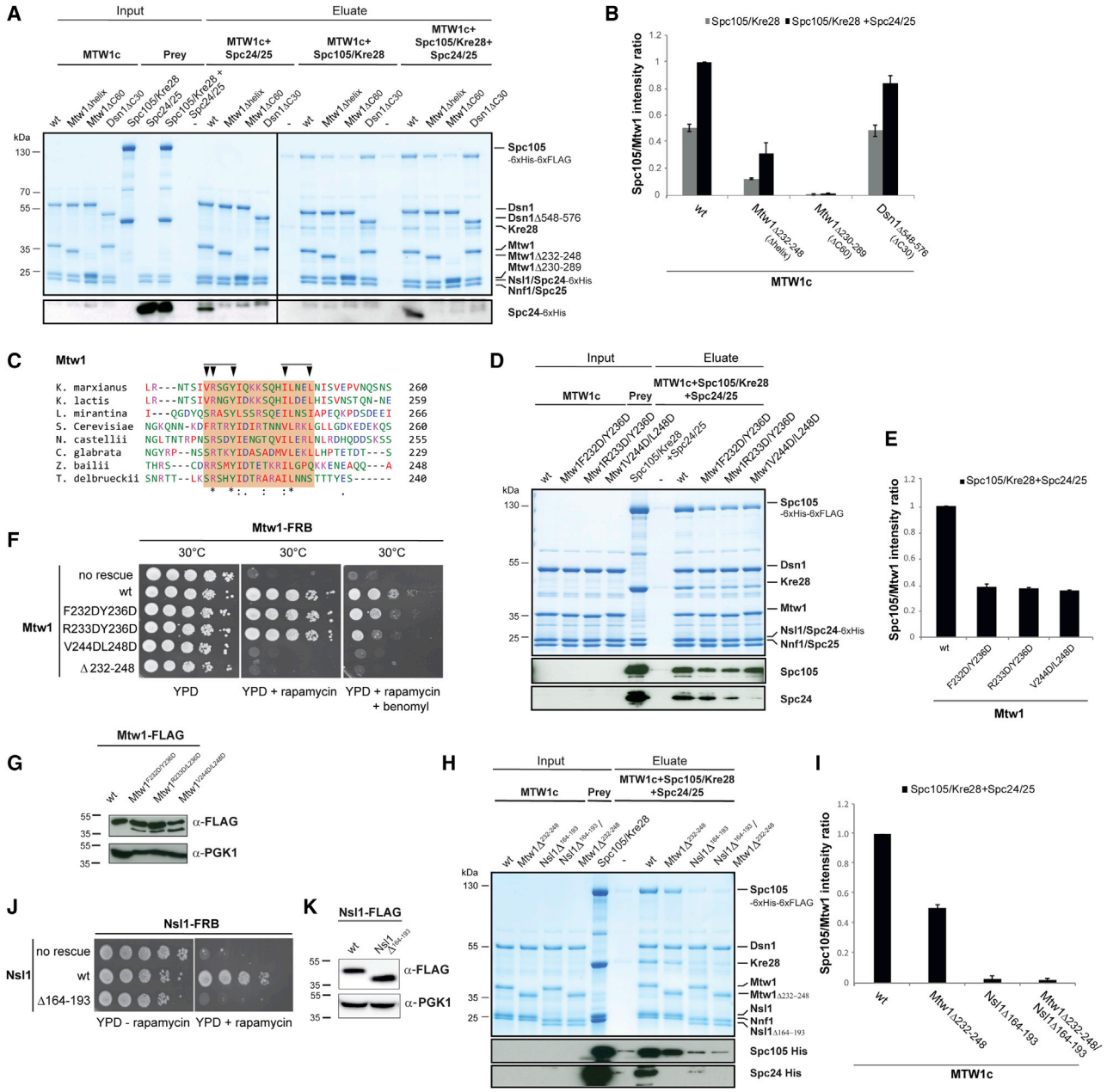

Figure 5. Cooperative Interactions between MTW1c C-Terminal Motifs and Spc24/25 and Spc105/Kre28 Complexes Stabilize the KMN Network

(A) The interaction of the Spc24/25 and/or Spc105/Kre28 complexes with C-terminal motifs of the MTW1c was assessed *in vitro*. Immobilized MTW1 wild-type and mutant complexes were incubated with either Spc24/25, Spc105/Kre28, or both. Bound complexes were eluted and analyzed by SDS-PAGE and Coomassie staining. Western blotting using anti-His antibody was performed to visualize the Spc24-6xHis levels.

(B) Quantification of bound Spc105 levels of the experiments described in (A) by measuring band intensities with ImageJ. The ratio of Spc105 to Mtw1 protein intensities was calculated as mean ± SD of 3 replicates.

(C) Amino acid sequence alignment of the Mtw1 helix$^{232–248}$ region from various budding yeast species. The predicted helical region of residues 232–248 in budding yeast is highlighted in pink. Amino acid residues are colored and annotated according to the Clustal Omega (Sievers et al., 2011) color and annotation codes. Arrowheads indicate the positions of the double mutations shown in (D) and (E).

(D) Double mutants of the Mtw1 helix$^{232–248}$ showed distinct effects on recruiting Spc24/25 or Spc105/Kre28 to the MTW1 complex *in vitro*. Mtw1 wild-type or Mtw1 mutant-containing complexes were incubated with Spc105/Kre28 and Spc24/25 at a molar ratio of 1:3, and experiments were analyzed as described in (A). The levels of Spc105-6xHis and Spc24-6xHis bound to the MTW1c were visualized by western blotting using the anti-His antibody.

(E) Quantification of the bound Spc105 levels relative to Mtw1 of the experiments in (D) (n = 2) as described in (B).

(legend continued on next page)

correlated with the loss of NDC80c binding *in vitro*, indicating that amino acids 244–248 of Mtw1 are necessary for Spc24/25 binding.

The Nsl1$^{163–192}$ Helical Motif Is Required for Recruiting the SPC105 and NDC80 Complexes

The peptide binding assay identified the Nsl1$^{163–192}$ motif to interact with Spc105/Kre28 (Figures 4C and 4D). We tested whether deletion of the Nsl1$^{164–193}$ helix in the recombinant MTW1c would affect binding of Spc105/Kre28 (Figures 5H and 5I). Deletion of the Nsl1$^{164–193}$ motif reduced Spc105/Kre28 levels associated with MTW1c to background levels and thus had a larger effect on Spc105/Kre28 binding than deletion of the Mtw1$^{233–248}$ helix. Consistent with the previous assay (Figure 5A), the deletion of the Mtw1$^{233–248}$ helix abrogated association with Spc24/25, but the MTW1cNsl1Δhelix$^{164–193}$ mutant retained minor Spc24/25 levels. As a direct interaction between the Nsl1$^{163–192}$ peptide and Spc24/25 was not detected (Figure 4A), its significant contribution to the recruitment of Spc24/25 to MTW1c may be a consequence of the lost cooperative stabilization through Spc105/Kre28 or may indicate a role in organizing the hub of C-terminal MTW1c motifs. Moreover, the Nsl1$^{163–192}$ motif was essential for cell viability (Figures 5J and 5K), which underscored its importance for the buildup of the KMN network.

A Kre28 CC Region Mediates Recruitment of Spc105/Kre28 to the MTW1 Complex

Our crosslink-derived subunit connectivity map of the native KMN network showed 4 and 12 crosslinks from the Mtw1 C terminus to Spc105 and Kre28 (Figure 1B), respectively. The majority of these crosslinks were detected at the transition of the C-terminal RWD domains to the flanking CC in Spc105 and close to the predicted C-terminal CC region in Kre28 (Figures 1B and 6A; Tables S4 and S5). In order to map the binding interface of MTW1c at the Spc105/Kre28 complex, we first deleted the Spc105 CC region (Δ551–711 "ΔCC") or the C terminus including the CC and RWD domains of Spc105 (Δ551–917 "ΔC") (Figure 6A). Both mutants did not support binding to the MTW1c (Figure 6B). Notably, these mutants also copurified significantly reduced levels of Kre28, which is in agreement with studies in higher eukaryotes (Kiyomitsu et al., 2011; Petrovic et al., 2010) and with inter-protein crosslinks connecting the CC regions of Spc105 and Kre28 (Figure 1B). This observation prompted us to test whether Kre28 itself is required for the interaction. We found that full-length Spc105 in the absence of Kre28 did not interact with the MTW1c, suggesting that Kre28 is required for recruiting Spc105/Kre28 to the MTW1c (Figure 6B).

The two predicted CCs of Kre28, Kre28$^{128–169}$ (CC1) and Kre28$^{229–259}$ (CC2) (Figure 6A), are connected by 20 crosslinks to the Spc105 CC region, Spc105$^{551–711}$ (Figure 1B; Tables S3 and S4), and 12 restraints linked Kre28$^{229–259}$ to the Mtw1 C terminus. We designed a series of double point mutants within CC1, Kre28$^{V136D/L139D}$ and Kre28$^{I143D/V146D}$, and CC2, Kre28$^{L231D/L234D}$, Kre28$^{L241D/L245D}$, and Kre28$^{M248D/V251D}$ (Figure 6C), which were copurified as stoichiometric complexes with Spc105 (Figures 6D and 6E). Mutations in CC1 did not affect interaction with MTW1c, whereas CC2 mutants retained either significantly reduced (Kre28$^{L231D/L234D}$) MTW1c levels or completely abrogated MTW1c binding (Kre28$^{L241D/L245D}$ and Kre28$^{M248D/V251D}$) (Figures 6D and 6E), suggesting that the predicted CC2 of Kre28 contributes to the recruitment of Spc105/Kre28 to the MTW1c.

To assess whether the Kre28 double point mutations were critical for the assembly of the KMN network *in vivo*, we ectopically expressed wild-type and mutant Kre28 proteins in *Kre28-FRB* anchor-away strains (Figures 6F and 6G). At 30°C, the Kre28 CC mutants showed wild-type growth, but at higher temperature mutations in CC1 abolished cell viability. This suggested that the CC1 and the CC2 were functionally distinct and indicated that the CC2 residues, which established the interaction between Spc105/Kre28 and MTW1c *in vitro*, were not essential *in vivo*. In order to perturb the integrity of the outer kinetochore, we deleted the non-essential CTF19c subunit Cnn1 (Bock et al., 2012; Pekgöz Altunkaya et al., 2016; Schleiffer et al., 2012). In a *Kre28-FRB/cnn1Δ* background, ectopic expression of the mutant Kre28 alleles showed only minor effects on cell growth at normal temperature. At higher temperature, the CC2 mutants, Kre28$^{L241D/L245D}$ and Kre28$^{M248D/V251D}$, which completely abrogated MTW1c binding *in vitro*, in contrast to Kre28$^{L231D/L234D}$ (Figures 6D and 6E), resulted in a severe growth defect (Figure 6F), indicating that these residues contribute to some extent to the stabilization of Spc105/Kre28 in the KMN network.

DISCUSSION

Our connectivity maps of the native and recombinant KMN network confirmed many known interactions that are required for recruiting the NDC80c to the CCAN (Figure 1B) and highlighted the recently described mode of NDC80c binding in humans and budding yeast through the Cnn1^{CENP-T}-Mcm16/Ctf3/Mcm22$^{CENP-H/I/K}$ pathway (Basilico et al., 2014; Bock et al., 2012; Huis In 't Veld et al., 2016; Lang et al., 2018; Pekgöz Altunkaya et al., 2016; Schleiffer et al., 2012).

Similar elongated structures were determined for the yeast and human MTW1^{MIS12} complexes (Dimitrova et al., 2016; Petrovic et al., 2016) with the N and C termini organized at opposite ends. The C termini were not proteolytically stable and thus not resolved in the structures (Dimitrova et al., 2016), indicating that

(F) Cell viability assay of the Mtw1 helix$^{232–248}$ double mutations using the anchor-away technique. Mtw1-FRB strains harboring the indicated rescue alleles were spotted in serial dilutions on YPD, YPD + rapamycin, or YPD + rapamycin + benomyl plates and incubated at 30°C or 37°C.
(G) Levels of the ectopically expressed Mtw1 proteins described in (E) are shown by western blotting.
(H) *In vitro* binding assay to investigate the interaction of the Spc105/Kre28 and Spc24/25 complexes with the MTW1c containing the Nsl1$^{Δ163–194}$ and Mtw1$^{Δ232–248}$ mutants. Experiments were performed as described in (A).
(I) Quantification of the bound Spc105 levels of the experiments in (H) (n = 2) as described in (B).
(J) Cell growth assay of the Nsl1$^{Δ163–194}$ mutant yeast cells. The Nsl1 wild-type and mutant proteins were ectopically expressed in a Nsl1-FRB strain, and cell growth was monitored by plating 1:10 serial dilutions on YPD medium at 30°C in the absence or presence of rapamycin.
(K) Levels of the ectopically expressed Nsl1 proteins described in (J) shown by western blotting.

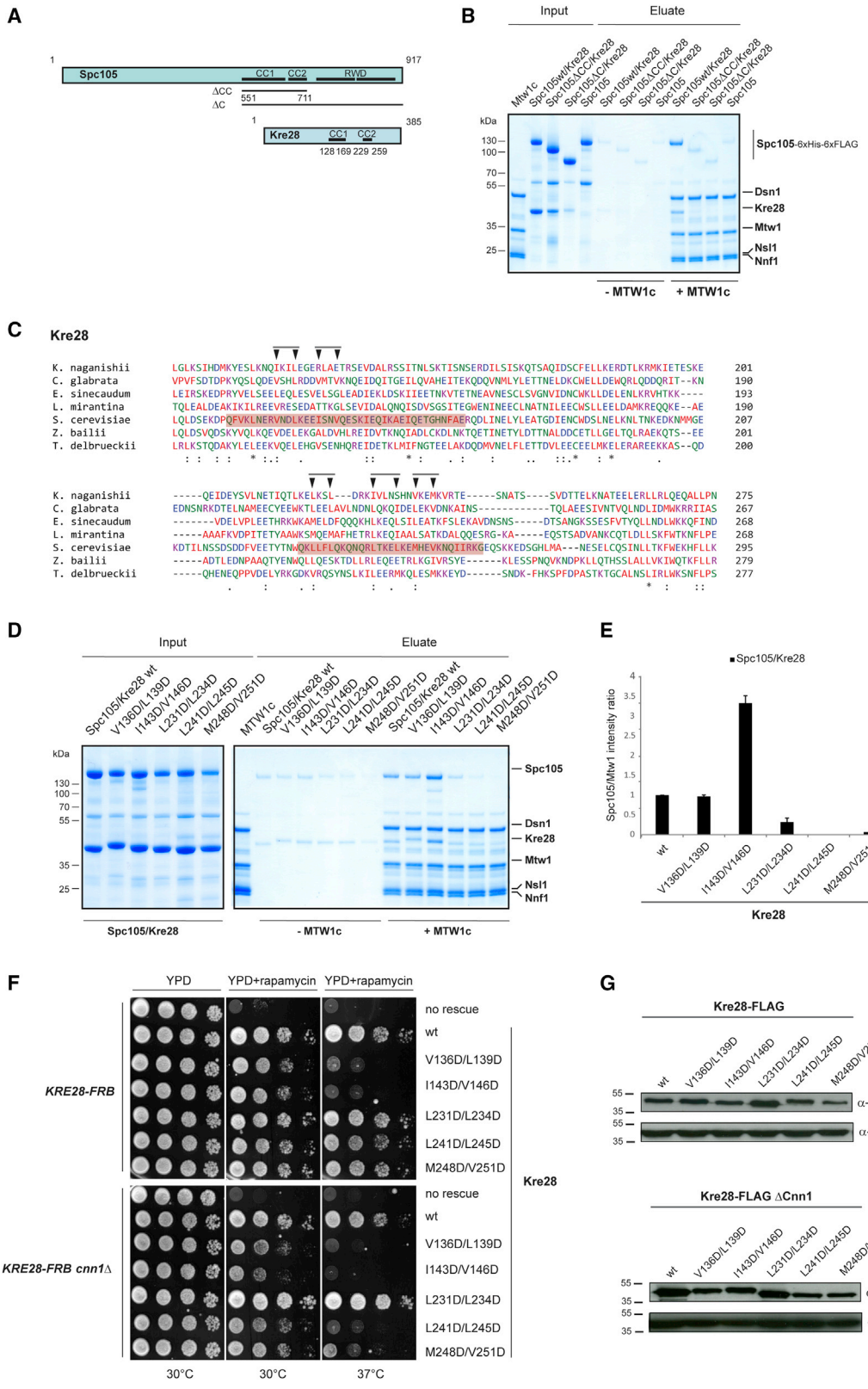

(legend on next page)

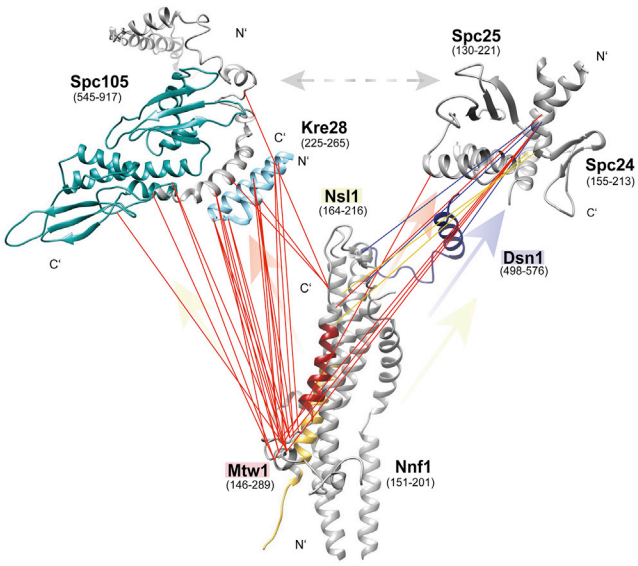

Figure 7. Crosslink Map Summarizing the Connectivity of the MTW1c C-Terminal Peptide Motifs with the Spc105/Kre28 and Spc24/25 Complexes

Models of Spc105/Kre28 and MTW1c were prepared using I-Tasser and Chimera, and the Spc24 and Spc25 C-terminal RWDs are represented by the crystal structure (PDB: 4GEQ) (Malvezzi et al., 2013). RWD domains of Spc105 (amino acids 545–917) are highlighted in cyan, and CC2 of Kre28 (amino acids 225–265) is shown in light blue. The partial model of MTW1c depicts the Mtw1 helix amino acids 232–248 (red), Nsl1 helix amino acids 164–193 (dark gold), and Dsn1 helix amino acids 547–576 (dark blue), with the accordingly colored crosslinks to Spc24/25 and Spc105/Kre28. The accordingly colored arrows indicate the binding dependencies detected in *in vitro* binding assays.

they are possibly stabilized upon binding to other KMN proteins. XL-MS analysis of the purified endogenous (Figure 1B) or the full-length recombinant KMN (Figure S1B) network showed that the crosslinks between the C termini of Mtw1, Dsn1, and Nsl1 are collinear (Figure 2A), suggesting that the tails are aligned in the KMN complex and create a hub for the interaction with the NDC80c and SPC105c.

Previous studies in yeast and humans identified the C-terminal tails of the MTW1c^{MIS12c} subunits as binding sites for the NDC80^{NDC80} and SPC105^{KNL1} complexes (Kudalkar et al., 2015; Malvezzi et al., 2013; Petrovic et al., 2010, 2014). In budding yeast, the NDC80c was shown to be recruited by the Dsn1 C terminus (Dimitrova et al., 2016; Malvezzi et al., 2013) and through interactions with the Mtw1 and Nsl1 C termini (Kudalkar et al., 2015). We found additional motifs and a hitherto underestimated role of Mtw1 and Nsl1 in KMN assembly (Figure 7). We identified a 17-amino acid helical motif (amino acids 232–248) in the Mtw1 C terminus required for binding to the Spc105/Kre28 complex and to the Spc24/25 heterodimer of the Ndc80 complex. Mutations of only two Mtw1 residues (V244D/L248D) in the tetrameric MTW1c, which did not affect association with Spc105/Kre28, resulted in loss of Spc24/25 binding and cell death (Figures 5D and 5F). Moreover, our findings *in vitro* and *in vivo* suggested that Mtw1$^{232–248}$ and Dsn1$^{548–576}$ cooperate in order to recruit NDC80c: (1) the binding of the MTW1 complex is completely abrogated by the Mtw1-Δhelix mutant despite the presence of a full-length Dsn1 protein, (2) Mtw1$^{232–248}$ and Dsn1$^{548–576}$ peptides synergistically increased the relative affinity to Spc24/25 (Figures 4A and 4B) in peptide binding assays and ITC experiments, and (3) the lethal phenotype observed upon deletion of the Mtw1 helix was not rescued by substituting the Mtw1 helix with the Cnn1$^{60–84}$ helix as it has been demonstrated by replacing the Dsn1$^{548–576}$ helix with Cnn1$^{60–84}$ (Figure 2D) (Malvezzi et al., 2013). Although Spc24/25 did not bind to the Nsl1$^{163–192}$ and Nsl1$^{183–216}$ peptides (Figure 4A), deletion of Nsl1$^{164–193}$ was lethal (Figure 5J) and abrogated binding of Spc24/25 to the MTW1c, suggesting that this Nsl1 motif might indirectly facilitate the Spc24/25 interaction (Figures 5H and 5I).

Apart from anchoring the outer kinetochore to the inner kinetochore through MTW1c^{MIS12c} and providing the microtubule binding site on NDC80c^{NDC80c}, the SPC105c^{KNL1c} of the KMN network serves as docking site for proteins of the spindle assembly checkpoint (Musacchio, 2015). In humans, the NSL1 C-terminal residues (258–281) interact with the homodimeric RWD domains of KNL1. The binding of NSL1 to KNL1 is only modestly enhanced by other members of the MIS12 complex, and the Kre28 ortholog ZWINT is dispensable for the interaction of KNL1c with MIS12c (Petrovic et al., 2010, 2014). Our results indicated that the recruitment of the Spc105/Kre28 complex in budding yeast differs from that of the human KMN network. First, the Mtw1$^{228–252}$ and the Nsl1$^{163–192}$ peptide bound Spc105/Kre28 *in vitro* (Figure 4C) and deletion of the individual motifs in the MTW1c severely affected the interaction (Figures 5A, 5B, 5H, and 5I), indicating that both motifs are required for stably tethering Spc105/Kre28. Second, the Spc105/Kre28 complex was recruited through Kre28 to the MTW1c. Moreover, the CC2 of Kre28 contributes to MTW1c binding, whereas CC1 is dispensable for this interaction (Figures 6D and 6E) and might be also functionally distinct from CC2 (Figure 6F). The role of

Figure 6. Recruitment of the Spc105/Kre28 Complex to the MTW1 Complex Is Mediated through Kre28

(A) Schematic representation of Spc105 and Kre28 deletion mutants studied in (B). ΔCC, delta coiled-coils (CC1 and CC2); ΔC, C-terminal truncation of amino acid residues 552–917.

(B) *In vitro* binding assay to study the interaction of the MTW1c with the indicated wild-type and mutant Spc105/Kre28 complexes including the various Kre28 mutants depicted in (A).

(C) Scheme of Kre28 double point mutants (arrowheads) in the CC1 (V136D/L139D, I143D/V146D) and CC2 (L231D/L234D, L241D/L245D, M248D/V251D) regions (highlighted in red orange).

(D) *In vitro* assay to investigate the binding of the MTW1c to the Spc105/Kre28 complexes carrying the Kre28 double point mutations shown in (C).

(E) Quantification of the Spc105 levels relative to Mtw1 of the experiments in (D) is displayed as mean ± SD (n = 2).

(F) Cell viability assay to test the Kre28 double point mutations applying the anchor-away technique. Cells ectopically expressing Kre28 wild-type and mutant proteins in the *KRE28-FRB* or *KRE28-FRB cnn1Δ* background were grown on YPD medium at 30°C or 37°C in the absence or presence or rapamycin.

(G) Western blot analysis of the Kre28 expression levels of the experiments shown in (F).

Kre28 has not been studied in detail, but its deletion is lethal in budding yeast (Pagliuca et al., 2009). Notably, Spc105/Kre28 bound the Cnn1$^{60–84}$ peptide *in vitro* (Figure 4C), which was also connected by a crosslink to the CC region of Spc105 (Figure 1B) in the endogenous KMN network. Whether this interaction is functionally relevant and contributes to outer kinetochore stabilization remains to be addressed.

Our peptide binding assays showed that equimolar mixtures of Mtw1$^{228–252}$ and Dsn1$^{548–576}$ or Mtw1$^{228–252}$ and Nsl1$^{163–192}$ cooperatively stabilized the association of Spc24/25 and Spc105/Kre28, respectively (Figures 4A and 4D). Although the individual Mtw1$^{228–252}$ and Dsn1$^{548–576}$ peptides, when simultaneously incubated with Spc105/Kre28 and Spc24/25, showed relatively weak affinity to Spc105/Kre28 and Spc24/25, respectively, the mixture of Mtw1$^{228–252}$ and Dsn1$^{548–576}$ peptides enriched a nearly stoichiometric super-complex of Spc105/Kre28 and Spc24/25 (Figure 4D). Similarly, the incubation of wild-type and mutant MTW1c with a mixture of Spc105/Kre28 and Spc24/25 increased the bound Spc105/Kre28 levels by 2-fold compared with incubation with Spc105/Kre28 alone (Figures 5A and 5B). These observations are consistent with a weak interaction of Spc105/Kre28 and Spc24/25 detected by SEC (Figure S3A) or by *in vitro* binding assay (Figure S3B). In humans, KNL1c and NDC80c independently interact with the MIS12c (Petrovic et al., 2010, 2014), whereas in *C. elegans* KNL1c is required for establishing a tight NDC80c-MIS12c interaction (Cheeseman et al., 2006). Whether the lack of cooperative stabilization of KNL1c and NDC80c on MIS12c is specific to the human KMN network, or whether this is the result of assays using truncated protein complexes, is unclear.

Using crosslink guided *in vitro* reconstitution (Figure 7), we identified distinct binding interfaces that cooperate in the stabilization of the NDC80c and SPC105c at the budding yeast KMN network, which may reflect the geometrical requirements of a kinetochore unit that transmits the tensile forces of a depolymerizing microtubule onto a single centromeric nucleosome. Whether cooperativity is established by similar subunit contacts within the human kinetochore, which is assembled at regional centromeres, and how post-translational modifications contribute to the formation of a high-affinity link between spindle microtubules and chromosomes will be exciting subjects of future research.

STAR★METHODS

Detailed methods are provided in the online version of this paper and include the following:

- KEY RESOURCES TABLE
- RESOURCE AVAILABILITY
  - Lead Contact
  - Materials Availability
  - Data and Code Availability
- EXPERIMENTAL MODEL AND SUBJECT DETAILS
- METHOD DETAILS
  - Plasmids and yeast strains
  - Yeast growth assays
  - Minichromosome loss assay
  - Purification of recombinant Spc24/25 and MTW1c
  - Purification of Spc105/Kre28 and KMN complexes
  - *In vitro* binding assays
  - Analytical size exclusion chromatography
  - Isothermal titration calorimetry
  - Sample preparation for native crosslinking analysis
  - Chemical crosslinking and mass spectrometry
  - Immunoprecipitation of the *in vivo* Mtw1 complex
  - Amino acid sequence alignment
  - Structural model prediction of KMN
- QUANTIFICATION AND STATISTICAL ANALYSIS

SUPPLEMENTAL INFORMATION

Supplemental Information can be found online at https://doi.org/10.1016/j.celrep.2020.108190.

ACKNOWLEDGMENTS

We thank Stefan Westermann for sharing reagents. J.F.-H., G.H., G.W., and F.H. were funded by the Research Training Group (GRK 1721), and M.P. and V.S.-M. were funded by the Graduate School (Quantitative Biosciences Munich) of the German Research Foundation (DFG). F.H. was supported by the European Research Council (ERC)-StG (638218), the Human Frontier Science Program (RGP0008/2015), the Bavarian Research Center of Molecular Biosystems, and an LMU excellent junior grant.

AUTHOR CONTRIBUTIONS

F.H. conceived the study. M.G.-S., M.P., T.Z., and J.F.-H. designed and executed the experiments with input from F.H. V.S.-M. helped with data analysis and bioinformatics. S.S. and T.S. cloned and provided recombinant proteins. G.H. assisted with data presentation. D.D. and G.W. performed the ITC experiments. M.G.-S., M.P., and F.H. wrote the manuscript.

DECLARATION OF INTERESTS

The authors declare no competing interests.

Received: February 12, 2020
Revised: July 18, 2020
Accepted: September 1, 2020
Published: September 29, 2020

REFERENCES

Akiyoshi, B., Sarangapani, K.K., Powers, A.F., Nelson, C.R., Reichow, S.L., Arellano-Santoyo, H., Gonen, T., Ranish, J.A., Asbury, C.L., and Biggins, S. (2010). Tension directly stabilizes reconstituted kinetochore-microtubule attachments. Nature *468*, 576–579.

Anedchenko, E.A., Samel-Pommerencke, A., Tran Nguyen, T.M., Shahnejat-Bushehri, S., Pöpsel, J., Lauster, D., Herrmann, A., Rappsilber, J., Cuomo, A., Bonaldi, T., and Ehrenhofer-Murray, A.E. (2019). The kinetochore module Okp1^{CENP-Q}/Ame1^{CENP-U} is a reader for N-terminal modifications on the centromeric histone Cse4^{CENP-A}. EMBO J. *38*, e98991.

Basilico, F., Maffini, S., Weir, J.R., Prumbaum, D., Rojas, A.M., Zimniak, T., De Antoni, A., Jeganathan, S., Voss, B., van Gerwen, S., et al. (2014). The pseudo GTPase CENP-M drives human kinetochore assembly. eLife *3*, e02978.

Bock, L.J., Pagliuca, C., Kobayashi, N., Grove, R.A., Oku, Y., Shrestha, K., Alfieri, C., Golfieri, C., Oldani, A., Dal Maschio, M., et al. (2012). Cnn1 inhibits the interactions between the KMN complexes of the yeast kinetochore. Nat. Cell Biol. *14*, 614–624.

Bodor, D.L., Mata, J.F., Sergeev, M., David, A.F., Salimian, K.J., Panchenko, T., Cleveland, D.W., Black, B.E., Shah, J.V., and Jansen, L.E. (2014). The quantitative architecture of centromeric chromatin. eLife *3*, e02137.

Cheeseman, I.M., and Desai, A. (2008). Molecular architecture of the kinetochore-microtubule interface. Nat. Rev. Mol. Cell Biol. *9*, 33–46.

Cheeseman, I.M., Enquist-Newman, M., Müller-Reichert, T., Drubin, D.G., and Barnes, G. (2001). Mitotic spindle integrity and kinetochore function linked by the Duo1p/Dam1p complex. J. Cell Biol. *152*, 197–212.

Cheeseman, I.M., Chappie, J.S., Wilson-Kubalek, E.M., and Desai, A. (2006). The conserved KMN network constitutes the core microtubule-binding site of the kinetochore. Cell *127*, 983–997.

Ciferri, C., Pasqualato, S., Screpanti, E., Varetti, G., Santaguida, S., Dos Reis, G., Maiolica, A., Polka, J., De Luca, J.G., De Wulf, P., et al. (2008). Implications for kinetochore-microtubule attachment from the structure of an engineered Ndc80 complex. Cell *133*, 427–439.

Cox, J., and Mann, M. (2008). MaxQuant enables high peptide identification rates, individualized p.p.b.-range mass accuracies and proteome-wide protein quantification. Nat. Biotechnol. *26*, 1367–1372.

De Wulf, P., McAinsh, A.D., and Sorger, P.K. (2003). Hierarchical assembly of the budding yeast kinetochore from multiple subcomplexes. Genes Dev. *17*, 2902–2921.

Dimitrova, Y.N., Jenni, S., Valverde, R., Khin, Y., and Harrison, S.C. (2016). Structure of the MIND Complex Defines a Regulatory Focus for Yeast Kinetochore Assembly. Cell *167*, 1014–1027.

Fischboeck, J., Singh, S., Potocnjak, M., Hagemann, G., Solis, V., Woike, S., Ghodgaonkar, M., Andreani, J., and Herzog, F. (2018). The COMA complex is required for positioning Ipl1 activity proximal to Cse4 nucleosomes in budding yeast. bioRxiv. https://doi.org/10.1101/444570.

Gascoigne, K.E., Takeuchi, K., Suzuki, A., Hori, T., Fukagawa, T., and Cheeseman, I.M. (2011). Induced ectopic kinetochore assembly bypasses the requirement for CENP-A nucleosomes. Cell *145*, 410–422.

Goshima, G., and Yanagida, M. (2000). Establishing biorientation occurs with precocious separation of the sister kinetochores, but not the arms, in the early spindle of budding yeast. Cell *100*, 619–633.

Grimm, M., Zimniak, T., Kahraman, A., and Herzog, F. (2015). xVis: a web server for the schematic visualization and interpretation of crosslink-derived spatial restraints. Nucleic Acids Res. *43* (*W1*), W362–W369.

Guimaraes, G.J., Dong, Y., McEwen, B.F., and Deluca, J.G. (2008). Kinetochore-microtubule attachment relies on the disordered N-terminal tail domain of Hec1. Curr. Biol. *18*, 1778–1784.

Haruki, H., Nishikawa, J., and Laemmli, U.K. (2008). The anchor-away technique: rapid, conditional establishment of yeast mutant phenotypes. Mol. Cell *31*, 925–932.

Herzog, F., Kahraman, A., Boehringer, D., Mak, R., Bracher, A., Walzthoeni, T., Leitner, A., Beck, M., Hartl, F.U., Ban, N., et al. (2012). Structural probing of a protein phosphatase 2A network by chemical cross-linking and mass spectrometry. Science *337*, 1348–1352.

Hieter, P., Mann, C., Snyder, M., and Davis, R.W. (1985). Mitotic stability of yeast chromosomes: a colony color assay that measures nondisjunction and chromosome loss. Cell *40*, 381–392.

Hinshaw, S.M., and Harrison, S.C. (2019). The structure of the Ctf19c/CCAN from budding yeast. eLife *8*, e44239.

Hornung, P., Maier, M., Alushin, G.M., Lander, G.C., Nogales, E., and Westermann, S. (2011). Molecular architecture and connectivity of the budding yeast Mtw1 kinetochore complex. J. Mol. Biol. *405*, 548–559.

Hornung, P., Troc, P., Malvezzi, F., Maier, M., Demianova, Z., Zimniak, T., Litos, G., Lampert, F., Schleiffer, A., Brunner, M., et al. (2014). A cooperative mechanism drives budding yeast kinetochore assembly downstream of CENP-A. J. Cell Biol. *206*, 509–524.

Huis In 't Veld, P.J., Jeganathan, S., Petrovic, A., Singh, P., John, J., Krenn, V., Weissmann, F., Bange, T., and Musacchio, A. (2016). Molecular basis of outer kinetochore assembly on CENP-T. eLife *5*, 5.

Janke, C., Magiera, M.M., Rathfelder, N., Taxis, C., Reber, S., Maekawa, H., Moreno-Borchart, A., Doenges, G., Schwob, E., Schiebel, E., and Knop, M. (2004). A versatile toolbox for PCR-based tagging of yeast genes: new fluorescent proteins, more markers and promoter substitution cassettes. Yeast *21*, 947–962.

Joglekar, A.P., Bloom, K., and Salmon, E.D. (2009). In vivo protein architecture of the eukaryotic kinetochore with nanometer scale accuracy. Curr. Biol. *19*, 694–699.

Jones, D.T. (1999). Protein secondary structure prediction based on position-specific scoring matrices. J. Mol. Biol. *292*, 195–202.

Kim, S., and Yu, H. (2015). Multiple assembly mechanisms anchor the KMN spindle checkpoint platform at human mitotic kinetochores. J. Cell Biol. *208*, 181–196.

Kiyomitsu, T., Murakami, H., and Yanagida, M. (2011). Protein interaction domain mapping of human kinetochore protein Blinkin reveals a consensus motif for binding of spindle assembly checkpoint proteins Bub1 and BubR1. Mol. Cell. Biol. *31*, 998–1011.

Kudalkar, E.M., Scarborough, E.A., Umbreit, N.T., Zelter, A., Gestaut, D.R., Riffle, M., Johnson, R.S., MacCoss, M.J., Asbury, C.L., and Davis, T.N. (2015). Regulation of outer kinetochore Ndc80 complex-based microtubule attachments by the central kinetochore Mis12/MIND complex. Proc. Natl. Acad. Sci. USA *112*, E5583–E5589.

Lampert, F., Mieck, C., Alushin, G.M., Nogales, E., and Westermann, S. (2013). Molecular requirements for the formation of a kinetochore-microtubule interface by Dam1 and Ndc80 complexes. J. Cell Biol. *200*, 21–30.

Lang, J., Barber, A., and Biggins, S. (2018). An assay for de novo kinetochore assembly reveals a key role for the CENP-T pathway in budding yeast. eLife *7*, e37819.

London, N., Ceto, S., Ranish, J.A., and Biggins, S. (2012). Phosphoregulation of Spc105 by Mps1 and PP1 regulates Bub1 localization to kinetochores. Curr. Biol. *22*, 900–906.

Malvezzi, F., Litos, G., Schleiffer, A., Heuck, A., Mechtler, K., Clausen, T., and Westermann, S. (2013). A structural basis for kinetochore recruitment of the Ndc80 complex via two distinct centromere receptors. EMBO J. *32*, 409–423.

Maskell, D.P., Hu, X.W., and Singleton, M.R. (2010). Molecular architecture and assembly of the yeast kinetochore MIND complex. J. Cell Biol. *190*, 823–834.

Miller, S.A., Johnson, M.L., and Stukenberg, P.T. (2008). Kinetochore attachments require an interaction between unstructured tails on microtubules and Ndc80(Hec1). Curr. Biol. *18*, 1785–1791.

Musacchio, A. (2015). The Molecular Biology of Spindle Assembly Checkpoint Signaling Dynamics. Curr. Biol. *25*, R1002–R1018.

Nishino, T., Rago, F., Hori, T., Tomii, K., Cheeseman, I.M., and Fukagawa, T. (2013). CENP-T provides a structural platform for outer kinetochore assembly. EMBO J. *32*, 424–436.

Pagliuca, C., Draviam, V.M., Marco, E., Sorger, P.K., and De Wulf, P. (2009). Roles for the conserved spc105p/kre28p complex in kinetochore-microtubule binding and the spindle assembly checkpoint. PLoS ONE *4*, e7640.

Pekgöz Altunkaya, G., Malvezzi, F., Demianova, Z., Zimniak, T., Litos, G., Weissmann, F., Mechtler, K., Herzog, F., and Westermann, S. (2016). CCAN Assembly Configures Composite Binding Interfaces to Promote Cross-Linking of Ndc80 Complexes at the Kinetochore. Curr. Biol. *26*, 2370–2378.

Petrovic, A., Pasqualato, S., Dube, P., Krenn, V., Santaguida, S., Cittaro, D., Monzani, S., Massimiliano, L., Keller, J., Tarricone, A., et al. (2010). The MIS12 complex is a protein interaction hub for outer kinetochore assembly. J. Cell Biol. *190*, 835–852.

Petrovic, A., Mosalaganti, S., Keller, J., Mattiuzzo, M., Overlack, K., Krenn, V., De Antoni, A., Wohlgemuth, S., Cecatiello, V., Pasqualato, S., et al. (2014). Modular assembly of RWD domains on the Mis12 complex underlies outer kinetochore organization. Mol. Cell *53*, 591–605.

Perez-Riverol, Y., Csordas, A., Bai, J., Bernal-Llinares, M., Hewapathirana, S., Kundu, D.J., Inuganti, A., Griss, J., Mayer, G., Eisenacher, M., et al. (2019). The

PRIDE database and related tools and resources in 2019: improving support for quantification data. Nucleic. Acids Res. *47*, 442–450.

Petrovic, A., Keller, J., Liu, Y., Overlack, K., John, J., Dimitrova, Y.N., Jenni, S., van Gerwen, S., Stege, P., Wohlgemuth, S., et al. (2016). Structure of the MIS12 Complex and Molecular Basis of Its Interaction with CENP-C at Human Kinetochores. Cell *167*, 1028–1040.

Pettersen, E.F., Goddard, T.D., Huang, C.C., Couch, G.S., Greenblatt, D.M., Meng, E.C., and Ferrin, T.E. (2004). UCSF Chimera–a visualization system for exploratory research and analysis. J. Comput. Chem. *25*, 1605–1612.

Pluta, A.F., Mackay, A.M., Ainsztein, A.M., Goldberg, I.G., and Earnshaw, W.C. (1995). The centromere: hub of chromosomal activities. Science *270*, 1591–1594.

Przewloka, M.R., Venkei, Z., Bolanos-Garcia, V.M., Debski, J., Dadlez, M., and Glover, D.M. (2011). CENP-C is a structural platform for kinetochore assembly. Curr. Biol. *21*, 399–405.

Rago, F., Gascoigne, K.E., and Cheeseman, I.M. (2015). Distinct organization and regulation of the outer kinetochore KMN network downstream of CENP-C and CENP-T. Curr. Biol. *25*, 671–677.

Santaguida, S., and Musacchio, A. (2009). The life and miracles of kinetochores. EMBO J. *28*, 2511–2531.

Schindelin, J., Arganda-Carreras, I., Frise, E., Kaynig, V., Longair, M., Pietzsch, T., Preibisch, S., Rueden, C., Saalfeld, S., Schmid, B., et al. (2012). Fiji: an open-source platform for biological-image analysis. Nat. Methods *9*, 676–682.

Schleiffer, A., Maier, M., Litos, G., Lampert, F., Hornung, P., Mechtler, K., and Westermann, S. (2012). CENP-T proteins are conserved centromere receptors of the Ndc80 complex. Nat. Cell Biol. *14*, 604–613.

Schneider, C.A., Rasband, W.S., and Eliceiri, K.W. (2012). NIH Image to ImageJ: 25 years of image analysis. Nat. Methods *9*, 671–675.

Screpanti, E., De Antoni, A., Alushin, G.M., Petrovic, A., Melis, T., Nogales, E., and Musacchio, A. (2011). Direct binding of Cenp-C to the Mis12 complex joins the inner and outer kinetochore. Curr. Biol. *21*, 391–398.

Shepperd, L.A., Meadows, J.C., Sochaj, A.M., Lancaster, T.C., Zou, J., Buttrick, G.J., Rappsilber, J., Hardwick, K.G., and Millar, J.B. (2012). Phosphodependent recruitment of Bub1 and Bub3 to Spc7/KNL1 by Mph1 kinase maintains the spindle checkpoint. Curr. Biol. *22*, 891–899.

Sievers, F., Wilm, A., Dineen, D., Gibson, T.J., Karplus, K., Li, W., Lopez, R., McWilliam, H., Remmert, M., Söding, J., et al. (2011). Fast, scalable generation of high-quality protein multiple sequence alignments using Clustal Omega. Mol. Syst. Biol. *7*, 539.

Spencer, F., Gerring, S.L., Connelly, C., and Hieter, P. (1990). Mitotic chromosome transmission fidelity mutants in Saccharomyces cerevisiae. Genetics *124*, 237–249.

van Hooff, J.J., Tromer, E., van Wijk, L.M., Snel, B., and Kops, G.J. (2017). Evolutionary dynamics of the kinetochore network in eukaryotes as revealed by comparative genomics. EMBO Rep. *18*, 1559–1571.

Walzthoeni, T., Claassen, M., Leitner, A., Herzog, F., Bohn, S., Förster, F., Beck, M., and Aebersold, R. (2012). False discovery rate estimation for cross-linked peptides identified by mass spectrometry. Nat. Methods *9*, 901–903.

Wei, R.R., Schnell, J.R., Larsen, N.A., Sorger, P.K., Chou, J.J., and Harrison, S.C. (2006). Structure of a central component of the yeast kinetochore: the Spc24p/Spc25p globular domain. Structure *14*, 1003–1009.

Wei, R.R., Al-Bassam, J., and Harrison, S.C. (2007). The Ndc80/HEC1 complex is a contact point for kinetochore-microtubule attachment. Nat. Struct. Mol. Biol. *14*, 54–59.

Weissmann, F., Petzold, G., VanderLinden, R., Huis In 't Veld, P.J., Brown, N.G., Lampert, F., Westermann, S., Stark, H., Schulman, B.A., and Peters, J.M. (2016). biGBac enables rapid gene assembly for the expression of large multisubunit protein complexes. Proc. Natl. Acad. Sci. USA *113*, E2564–E2569.

Westermann, S., Cheeseman, I.M., Anderson, S., Yates, J.R., 3rd, Drubin, D.G., and Barnes, G. (2003). Architecture of the budding yeast kinetochore reveals a conserved molecular core. J. Cell Biol. *163*, 215–222.

Westermann, S., Wang, H.W., Avila-Sakar, A., Drubin, D.G., Nogales, E., and Barnes, G. (2006). The Dam1 kinetochore ring complex moves processively on depolymerizing microtubule ends. Nature *440*, 565–569.

Xiao, H., Wang, F., Wisniewski, J., Shaytan, A.K., Ghirlando, R., FitzGerald, P.C., Huang, Y., Wei, D., Li, S., Landsman, D., et al. (2017). Molecular basis of CENP-C association with the CENP-A nucleosome at yeast centromeres. Genes Dev. *31*, 1958–1972.

Yamagishi, Y., Yang, C.H., Tanno, Y., and Watanabe, Y. (2012). MPS1/Mph1 phosphorylates the kinetochore protein KNL1/Spc7 to recruit SAC components. Nat. Cell Biol. *14*, 746–752.

Yang, J., Yan, R., Roy, A., Xu, D., Poisson, J., and Zhang, Y. (2015). The I-TASSER Suite: protein structure and function prediction. Nat. Methods *12*, 7–8.

Zimmermann, L., Stephens, A., Nam, S.Z., Rau, D., Kübler, J., Lozajic, M., Gabler, F., Söding, J., Lupas, A.N., and Alva, V. (2018). A Completely Reimplemented MPI Bioinformatics Toolkit with a New HHpred Server at its Core. J. Mol. Biol. *430*, 2237–2243.

STAR★METHODS

KEY RESOURCES TABLE

REAGENT or RESOURCE	SOURCE	IDENTIFIER
Antibodies		
Mouse monoclonal anti-6xHis tag	ABCAM	Cat# ab18184; RRID:AB_444306
Mouse monoclonal anti-FLAG M2	Sigma-Aldrich	Cat# F1804; RRID:AB_262044
Mouse monoclonal anti-Pgk1	Invitrogen	Cat# 459250; RRID:AB_2532235
Goat anti-mouse IgG-HRP	Santa Cruz Biotechnology	Cat# sc-2005; RRID:AB_631736
Bacterial and Virus Strains		
E. coli: BL21 (DE3)	New England Biolabs	Cat#C2527
E. coli: DH10Bac	ThermoFisher	Cat#10361012
Chemicals, Peptides, and Recombinant Proteins		
BS3-H12/D12 crosslinker	Creative Molecules	Cat#001SS
TCEP	ThermoFisher	Cat#20490
Iodoacetamide	Sigma-Aldrich	Cat#I6125
Lysyl Endopeptidase	FUJIFILM Wako Pure Chemical Corporation	Cat#125–05061
Trypsin Sequencing Grade Modified	Promega	Cat#V5111
Rapamycin	Invitrogen	Cat#PHZ1235
Benomyl	Sigma-Aldrich	Cat#381586
FuGENE HD Transfection Reagent	Sigma-Aldrich	Cat#E2311
cOmplete ULTRA EDTA-free Protease Inhibitor Cocktail	Roche	Cat#5892953001
Ni-NTA Agarose	QIAGEN	Cat#30210
Strep-Tactin Superflow Plus Agarose	QIAGEN	Cat#30004
anti-FLAG M2 agarose	Sigma-Aldrich	Cat#A2220
Peptides listed in Table S3	Ontores	N/A
Mtw1 complex	this paper	N/A
Spc24/25	this paper	N/A
Spc105/Kre28	this paper	N/A
KMN complex	this paper	N/A
Critical Commercial Assays		
Q5 Site-Directed Mutagenesis Kit	New England Biolabs	Cat#E0552S
Mini-prep kit	QIAGEN	Cat#27104
Deposited Data		
PRIDE, *in vivo* network	Perez-Riverol et al., 2019	PXD011774
PRIDE, *in vitro* reconstituted KMN	Perez-Riverol et al., 2019	PXD011775
Experimental Models: Cell Lines		
S. frugiperda: SF21	ThermoFisher	Cat#11497013
Trichoplusia ni: High five	ThermoFisher	Cat#B85502
Experimental Models: Organisms/Strains		
E. coli: BL21 (DE3)	New England Biolabs	Cat#C2527
E. coli: DH10Bac	ThermoFisher	Cat#10361012
S. cerevisiae: S288c listed in Table S1		N/A
Recombinant DNA		
pETDuet-1 vector	Novagen	Cat#71146-3
pETDuet-1 Spc24-6xHis-Spc25	this paper	N/A

(*Continued on next page*)

Continued

REAGENT or RESOURCE	SOURCE	IDENTIFIER
pKP-29	Gift from Hopfner Lab	N/A
pKP29-6xHis-1xStrep-Dsn1Δ2-171-Nsl1-Nnf1-Mtw1 (mutants listed in Table S2)	this paper	N/A
pLIB	Weissmann et al., 2016	Addgene #80610
Spc105-6xFlag-6xHis-Kre28 (mutants listed in Table S2)	this paper	N/A
pBIG2ABC	Weissmann et al., 2016	Addgene # 80617
pBIG2ABC Ndc18-Nuf2-Spc24-Spc25-Mtw1-Nnf1-Nsl1-Dsn1-Spc105-6xHis6xFlag-Kre28	this paper	N/A
pYCF1/ CEN3.L	Nasmyth Lab	N/A
Software and Algorithms		
xQuest	Walzthoeni et al., 2012	
xVis	Grimm et al., 2015	https://xvis.genzentrum.lmu.de/login.php
MaxQuant	Cox and Mann, 2008	https://www.maxquant.org/
Clustal Omega	Sievers et al., 2011	https://www.ebi.ac.uk/Tools/msa/clustalo/
BLAST	NCBI	https://blast.ncbi.nlm.nih.gov/Blast.cgi
I-Tasser	Yang et al., 2015	https://zhanglab.ccmb.med.umich.edu/I-TASSER/
UCSF Chimera	Pettersen et al., 2004	http://www.cgl.ucsf.edu/; Pettersen et al., 2004
PSIPRED	Jones, 1999	http://bioinf.cs.ucl.ac.uk/psipred/
HHpred	Zimmermann et al., 2018	https://toolkit.tuebingen.mpg.de/tools/hhpred
ImageJ	Schindelin et al., 2012	https://imagej.nih.gov/ij/
Other		
Sep-Pak tC18 cartridges	Waters	Cat#WAT054960
PD-10 Desalting Columns	GE Healthcare	Cat#17085101

RESOURCE AVAILABILITY

Lead Contact

Further information and requests for resources and reagents should be directed to and will be fulfilled by the Lead Contact, Franz Herzog (herzog@genzentrum.lmu.de).

Materials Availability

All unique/stable reagents generated in this study are available from the Lead Contact on request.

Data and Code Availability

The mass spectrometry data reported in this paper have been deposited to the ProteomeXchange Consortium via the PRIDE partner repository. The accession number for the endogenous KMN XL-MS data is PRIDE: PXD011774 and for the recombinant KMN XL-MS data is PRIDE: PXD011775.

EXPERIMENTAL MODEL AND SUBJECT DETAILS

Genes used for expression of recombinants proteins were PCR amplified from *S. cerevisiae* gDNA. *E. coli* BL21 (DE3) cells were grown in LB media on 18°C or 37°C. Yeast strains were grown in yeast extract/peptone or synthetic media [without Histidine (SD - His), without Uracil (SD - Ura), or both (SD - His - Ura) and with all amino acids but low (6 μg/ml) adenine (SD complete)]. Cells were typically incubated at 30°C unless otherwise indicated

METHOD DETAILS

Plasmids and yeast strains

All plasmids and yeast strains used in this study are listed in Tables S1 and S2, respectively. For protein expression in *E. coli*, cDNAs of Spc24 and Spc25 were cloned into pETDuet-1 (Novagen) using NcoI/BamHI in sequence with the C-terminal 6xHis tag and NdcI/KpnI, respectively. 6xHis1xStrepDsn1$^{\Delta 2\text{-}171}$/Nsl1/Nnf1/Mtw1 genes were sequentially cloned with AscI/AarI sites into the pKP-29 polycistronic vector cut with AscI/NotI (Table S2). Open reading frames (ORFs) encoding the Spc105-6xHis6xFLAG and Kre28 subunits were amplified from yeast genomic DNA and cloned into the pBIG1 vector according to the biGBac system (Weissmann et al., 2016). Similarly, Dsn1/Nsl1/Nnf1/Mtw1 and Ndc80/Nuf2/Spc24/25 ORFs were amplified and subsequently cloned into pBIG1 plasmids. The KMN network complex was assembled in a pBIG2 vector. Mtw1, Nsl1 and Kre28 mutants were generated using the Q5 mutagenesis kit (New England Biolabs). Constructs were sequence verified.

Yeast strains were created in the S288C background (Table S1). Epitope tags were inserted at the 3′ ends of genes at their native loci by a PCR based tagging standard approach (Janke et al., 2004). The anchor-away technique of Mtw1 mutants (Mtw1-FRB) was performed by endogenously tagging the FRB domain to the Mtw1 in a strain expressing the ribosomal RPL13-FKBP12 anchor. The Mcm21-FRB strain was created similarly (Haruki et al., 2008). For Mtw1 anchor away and rescue experiments, we cloned the 5′ UTR region (200 bp) with the Mtw1-1xFLAG into the pRS313 vector. C-terminal gene truncations were made with the Q5® Site-Directed Mutagenesis Kit (NEB). The sectoring assay plasmid (2886) used in this study was pYCF1/ CEN3. The Mtw1 rescue and sectoring assay plasmids were co-transformed into the Mtw1 anchor-away strain and selected on SD – His – Ura plates. Anchor-away rescue experiments for *Dsn1-1xFLAG* or *Kre28-1xFLAG* were performed in the same manner. The cell growth was tested on YPD plates in the absence or presence of rapamycin.

Yeast growth assays

To test the temperature and benomyl sensitivity of anchor-away strains ectopically expressing wild-type and mutant proteins, cells were grown overnight in YPD broth at 30°C. 2.5 μL of five 10-fold serial dilutions starting at OD_{600} = 0.5 were spotted on YPD plates, YPD + rapamycin (1 μg/ml, Invitrogen) and YPD + rapamycin + benomyl (15 μg/ml,Merck) plates. Plates were incubated at 30°C or 37°C for 3-5 days.

Minichromosome loss assay

The sectoring assay was performed as described (Spencer et al., 1990), ensuring that the cultures were first grown overnight in SD – His – Ura media that selected for SUP11 plasmid and Mtw1 mutant constructs. An aliquot (OD600 0.5) was harvested and the pellet was resuspended in 100 μl aqua dest. 200 μl of a 1:10000 dilution was plated on SD complete low Ade, SD complete low Ade + rapamycin (1 μg/ml) and SD complete low Ade + rapamycin + benomyl (15 μg/ml) plates. The plates were incubated at 30°C for 3 days. The percent of red or sectored versus completely white colonies was scored. A Mcm21-FRB strain served as a positive control. The experiments were performed at least three times and an average with the standard deviation was calculated for each strain.

Purification of recombinant Spc24/25 and MTW1c

For Spc24-6xHis/Spc-25 or MTW1c (6xHis-1xStrep-Dsn1$^{\Delta 2\text{-}171}$/Nsl1/Nnf1/Mtw1 or mutants thereof listed in Table S2) expression, bacteria were grown to an OD_{600} of 0.6 at 37°C and protein expression was induced with 0.2 mM (Spc24-6xHis/25) or 0.5 mM (MTW1c) IPTG overnight at 18°C. Cells were lysed in lysis buffer (30 mM HEPES, pH 7.5, 300 mM NaCl, 5% glycerol, 30 mM imidazole, 0.02% Tween, 5% glycerol, Complete EDTA-free protease inhibitors [Roche]) using a M-110L Microfluidizer (Microfluidics). The cleared lysate was incubated with Ni-NTA agarose beads (QIAGEN). The protein complexes were eluted with buffer containing 30 mM HEPES (pH 7.5), 150 mM NaCl, 0.01% Tween, 3% glycerol and 250 mM imidazole. The Spc24/25 complex was further purified on a Superdex 200 HiLoad 16/60 column (GE Healthcare) in a buffer containing 30 mM HEPES (pH 7.5), 150 mM NaCl and 3% glycerol.

Purification of Spc105/Kre28 and KMN complexes

Viruses were generated by transfection of Sf21 insect cells (Thermo Scientific) with the recombinant baculoviral genome using FuGENE HD transfection reagent (Promega). Protein complexes were expressed in High Five (Thermo Scientific) insect cell suspension cultures.

For purification of Spc105/Kre28 and KMN complexes, insect cells were lysed in lysis buffer (50 mM Tris, pH 7.5, 150 mM NaCl, 5% glycerol, Complete EDTA-free protease inhibitors [Roche]) using a Dounce homogenizer. Cleared extracts were incubated with M2 anti-FLAG agarose (Sigma-Aldrich) for 1 h, washed 3x with lysis buffer and eluted in lysis buffer containing 1 mg/ml 3xFLAG peptide and 10% glycerol.

In vitro binding assays

For peptide binding analysis recombinant Spc24/25 or Spc105/Kre28 complexes were incubated with a 25-fold molar excess of 1xStrep-tagged peptides (Table S3) in binding buffer (30 mM HEPES pH 8, 150 or 300 mM NaCl, 5% glycerol and 0.02% NP40) and incubated at 25°C/1000 rpm for 30 minutes using a thermomixer (Eppendorf). The protein complexes were bound to Strep-Tactin

Superflow agarose (QIAGEN) at 1000 rpm and room temperature for 30 min. The immobilized protein complexes were washed twice with binding buffer and eluted in 30 mM HEPES (pH 8), 500 mM NaCl, 5% glycerol, 0.02% NP40 and 8 mM biotin.

For binding assays using Mtw1 protein complexes, Mtw1 complex purified via 6xHis tag and eluted in imidazole (described above) was concentrated on Strep-Tactin Superflow agarose (QIAGEN) and washed with Strep-wash buffer (30 mM HEPES pH 7.5, 150 mM NaCl, 5% glycerol, 0.01% Tween 20). The immobilized MTW1c was incubated with the various protein complexes in a 1:3 ratio for 30 minutes in a thermomixer (Eppendorf) at 1200 rpm and 4°C and washed with Strep-high salt wash buffer (30 mM HEPES pH 7.5, 300 mM NaCl, 5% glycerol, 0.02% Tween 20). The complexes were eluted in 30 mM HEPES pH 8.0, 150 mM NaCl, 5% glycerol and 8 mM biotin. Proteins were resolved on 10%–15% gradient SDS-PAGE gels and stained with Coomassie Brilliant Blue G250 (Roth). Immunoblotting for Spc24-6xHis was performed using mouse anti-6xHis tag (1:1000, ABCAM) and visualized with goat anti-mouse HRP -conjugated secondary antibody (1:15000, Santa Cruz).

Analytical size exclusion chromatography

Analytical size exclusion chromatography was performed on a Superose 6 Increase 3.2/300 column (GE Healthcare). Proteins were mixed in an equimolar ratio and incubated for 1 h on ice. Samples were eluted under isocratic conditions at 4°C in a buffer containing 50 mM HEPES pH 7.5, 180 mM NaCl, 3% glycerol. Elution of proteins was monitored by absorbance at 280 nm. 100 µl fractions were collected and analyzed by SDS-PAGE and Silver staining.

Isothermal titration calorimetry

ITC experiments were performed using a PEAQ-ITC system (Malvern) with 51 µM of Spc24-6xHis/25 in 30 mM HEPES (pH 7.5), 150 mM NaCl and 5% glycerol in the cell. 800 µM of Dsn1$^{555-574}$ or Dsn1$^{555-574}$-Mtw1$^{229-251}$ peptide (Table S3) were titrated into the cell in 13 individual injections of 3 µl, spaced 150 s apart at 25°C. Data evaluation was performed with the Malvern software package. Experiments were performed in triplicates to confirm the robustness of the assay.

Sample preparation for native crosslinking analysis

A PCR-based approach was used for tagging Dsn1, Mcm16, Ctf3, Cnn1, and Wip1 with 6xHis-6xFLAG at the endogenous loci in a DDY1810 (protease deficient) background. Cells were grown in YPD medium in 5 l flasks for initial tests or in a 300 l fermenter (Bioengineering) for preparative kinetochore purifications. Cell pellets were resuspended in lysis buffer (25 mM HEPES pH 8, 150 mM KCl, 5% glycerol, 2 mM $MgCl_2$, 0.02% NP-40) and droplets of yeast cell suspension were flash-frozen in liquid nitrogen and subsequently grinded into powder by a SPEX SamplePrep 970EFM freezer mill (C3 Prozess- und Analysentechnik GmbH). For protein complex purification 200 g of frozen cell powder were dissolved in 90 mL lysis buffer supplemented with phosphatase (Thermo Fisher Scientific) and protease inhibitors (Protease Inhibitors Cocktail Mix IV, Merck). Whole cell lysates were incubated with 120 U/ml benzonase (Sigma-Aldrich) for 30 min at room temperature and centrifuged at 65000 x g for 30 min. Tagged kinetochore subunits were immunoprecipitated by incubating cleared lysates with Protein A Dynabeads (Life Technologies) coupled to anti-FLAG M2 antibody (Sigma-Aldrich). Beads were washed once with 50 mL and once with 25 mL lysis buffer. Bound protein complexes were eluted from the magnetic beads using 0.15 mg/ml 2xStrep-6xFLAG peptide. Excess of peptide was removed by passing the eluate over a Strep-Tactin column (QIAGEN). For chemical crosslinking the eluted complexes were re-isolated on a Ni-NTA (QIAGEN) matrix.

Chemical crosslinking and mass spectrometry

Purified native and *in vitro* reconstituted kinetochore complexes were crosslinked by resuspending protein bound beads in an equimolar mixture of isotopically light (hydrogen) and heavy (deuterium) labeled bis[sulfosuccinimidyl]suberate (BS3, H_{12}/D_{12}) (Creative Molecules) at a final concentration of 0.25 - 0.5 mM at 30°C for 30 min. The crosslinking reaction was quenched by adding ammonium bicarbonate to a final concentration of 100 mM for 20 min at 30°C. The chemical crosslinks on native kinetochore complexes were identified by mass spectrometry as previously described (Walzthoeni et al., 2012). Briefly, crosslinked complexes were reduced with 5 mM TCEP (Thermo Fisher Scientific) at 35°C for 15 min and alkylated with 10 mM iodoacetamide (Sigma-Aldrich) at room temperature for 30 min in the dark. Proteins were digested with Lys-C (1:50 (w/w), Wako Pure Chemical Industries) at 35°C for 3 h, diluted with 50 mM ammonium bicarbonate to 1 M urea, and digested with trypsin (1:50 (w/w), Promega) overnight. Peptides were acidified with trifluoroacetic acid (TFA) at a final concentration of 1% and purified by reversed phase chromatography using C18 cartridges (Sep-Pak, Waters). Crosslinked peptides were enriched on a Superdex Peptide PC 3.2/30 column using water/acetonitrile/TFA (75/25/0.1, v/v/v) as mobile phase at a flow rate of 50 µl/min and were analyzed by liquid chromatography coupled to tandem mass spectrometry (LC-MS/MS) using an Orbitrap Elite instrument (Thermo Fisher Scientific). Fragment ion spectra were searched and crosslinks were identified by the dedicated software *xQuest* (Walzthoeni et al., 2012). The results were filtered according to the following parameters: Δ score $\leq$ 0.85, MS1 tolerance window of -4 to 4 ppm and score $\geq$ 22. The quality of all crosslink spectra passing the filter was manually validated and crosslinks were visualized as network plots using the webserver *xVis* (Grimm et al., 2015). The mass spectrometry proteomics data have been deposited to the ProteomeXchange Consortium via the PRIDE (Perez-Riverol et al., 2019) partner repository with the dataset identifier PXD011774 (in vivo network) and PXD011775 (*in vitro* reconstituted KMN).

Immunoprecipitation of the *in vivo* Mtw1 complex

Mtw1 anchor-away strains YTZ83-YTZ88 (Table S1) ectopically expressing Mtw1 wild-type and mutant proteins from rescue plasmids were grown at 30°C in 50 mL SD(-)His + 2% dextrose medium to an OD_{600} of 1-1.5. The cell density was normalized to the same OD_{600} and cells were pelleted and frozen as droplets in liquid N_2 and homogenized using a freezer mill.

For immunoprecipitation assays, 0.25-1 g of yeast powder were resuspended in IP buffer with protease inhibitors (25 mM HEPES pH 7.5, 150 mM KCl, 0.08% NP-40, 1 mM EDTA, 5 mM EGTA, 2 mM $MgCl_2$, 1.5x protease- [Calbiochem] and HALT phosphatase inhibitor cocktail [Thermo Fisher Scientific]) and lysed by intermittent vortexing and incubation on ice using 500 μL glass beads (0.5 mm diameter, Microspec). Lysates were cleared at 21000 x g for 30 minutes. 20 μL of anti-FLAG M2 agarose (Sigma-Aldrich) were incubated with the lysate at 4°C for one hour. Beads were washed once with 1 mL of IP buffer and once with wash buffer (25 mM HEPES pH 7.5, 150 mM KCl, 0.008% NP-40, 1 mM EDTA, 5 mM EGTA, 2 mM $MgCl_2$). Mtw1 proteins were eluted in wash buffer containing 0.5 mg/ml 3xFLAG peptide. Samples were analyzed using 4%–20% gradient SDS-PAGE gels (Mini-PROTEAN TGX, BioRad), immunoblotted using anti-FLAG M2 (1:5000, Sigma-Aldrich) and anti-Pgk1 (1:10000, Invitrogenantibodies, and visualized by the HRP-conjugated anti mouse secondary antibody (1:10000, Santa Cruz).

For mass spectrometric analysis, 5-20 g of yeast powder was lysed and Mtw1-1xFLAG purification was performed as described above. The eluates were subjected to tryptic digestion using the protocol described in the section above, and the tryptic peptides were separated from the 3xFLAG peptide by size exclusion chromatography. Samples were analyzed by LC-MS/MS using an Orbitrap Elite instrument (Thermo Fisher Scientific).

Protein intensities obtained by the software suite MaxQuant (Cox and Mann, 2008) of 5 biological replicates were extracted and merged by protein name. The least correlated replicate was removed and thus, 4 replicates per Mtw1 variant were analyzed. Proteins detected in a single replicate were eliminated and single peptide identifications present in at least 3 replicates were included. Protein raw intensities were normalized to the peptide count and log2-transformed. To penalize the lack of reproducibility, not detected protein intensity values in replicates were set to the minimum abundance in the matrix minus an offset. The average ratios of interactor to bait intensities were calculated and displayed by a color scale.

Amino acid sequence alignment

Interrelated budding yeast species with the highest similarity to *S. cerevisiae* Mtw1 or Kre28 protein were determined by a protein BLAST search. Multiple sequence alignments of Mtw1 and Kre28 protein sequences were conducted using Clustal Omega (Sievers et al., 2011).

Structural model prediction of KMN

Individual models were predicted using I-Tasser (Yang et al., 2015). The template for the MTW1c C-terminal region was specified without alignment using crystallized *K. lactis* MTW1c (PDB entry 5T58) (Dimitrova et al., 2016). The alignment of individual proteins was performed in UCSF Chimera (Pettersen et al., 2004) applying the match maker tool. Spc105 was modeled using the crystal structure of human Knl1 (PDB entry 4NF9) (Petrovic et al., 2014). The Kre28 model was obtained without a template.

QUANTIFICATION AND STATISTICAL ANALYSIS

Statistical analyses are described in the Figure legends and the Method Details.